ENGINEERING-PDH.com
ONLINE CONTINUING EDUCATION

EFFICIENT STRESS TRANSFER IN BINARY PARTICLE SYSTEMS

Main Category:	Materials Engineering
Sub Category:	-
Course #:	MAT-122
Course Content:	91 pgs
PDH/CE Hours:	7

OFFICIAL COURSE/EXAM

(SEE INSTRUCTIONS ON NEXT PAGE)

WWW.ENGINEERING-PDH.COM
TOLL FREE (US & CA): 1-833-ENGR-PDH (1-833-364-7734)
SUPPORT@ENGINEERING-PDH.COM

MAT-122 EXAM PREVIEW

- TAKE EXAM! -

Instructions:

- At your convenience and own pace, review the course material below. When ready, click "Take Exam!" above to complete the live graded exam. (Note it may take a few seconds for the link to pull up the exam.) You will be able to re-take the exam as many times as needed to pass.
- Upon a satisfactory completion of the course exam, which is a score of 70% or better, you will be provided with your course completion certificate. Be sure to download and print your certificates to keep for your records.

Exam Preview:

1. Traditional methods for determining stresses (i.e., Boussinesq's equation for soils) require treating the particulate system as an idealized homogeneous, elastic, and isotropic system. Most particulate systems, in particular soils, deviate from these idealizations often resulting in calculation errors of 25 to 30 percent.
    a. True
    b. False
2. According to the reference material, a blend with greater than __ percent coarse material behaves as a uniformly coarse material.
    a. 50
    b. 60
    c. 70
    d. 80
3. The DEM is an iterative, cyclic calculation numerical model. The force and moment sums are used to compute the linear and rotational accelerations of each particle, which are numerically integrated to yield velocity, and integrated again to give displacement according to Newton's third law of motion.
    a. True
    b. False
4. According to the reference material, blends with less than __ percent coarse material behave as a uniformly fine material.
    a. 30
    b. 40
    c. 50
    d. 60

5. As of this study, due to the computational time requirements, only a few tens of thousands of particles can be simulated on a personal computing platform. Simulation of field applications using the same sand would require well over _____ particles.
    a. 250,000
    b. 500,000
    c. 1 million
    d. 1 billion
6. Consolidated-undrained triaxial compression testing conducted in accordance with ASTM D 4767 (ASTM 2004) provides data on the strength and stress-strain relationship of a cylindrical particulate specimen.
    a. True
    b. False
7. According to the reference material, rigid objects can move through 3 linear displacement and ___ rotational degrees of freedom.
    a. 3
    b. 4
    c. 5
    d. 6
8. According to the reference material, type ___ stainless steel is used widely in anti-friction applications where high hardness and corrosion resistance are required.
    a. 430F
    b. 440A
    c. 316L
    d. 440C
9. According to the reference material, A state of stress equilibrium is approached at both 15 and 50 psi for the stainless-steel assemblies blended at or near 50-50 and the polypropylene/stainless steel assemblies blended at __-__.
    a. 49-51
    b. 48-52
    c. 45-55
    d. 40-60
10. According to the reference material, during triaxial compression testing, the coordination number increased slightly for the bimodal distributions, but more significantly for the uniform assemblies.
    a. True
    b. False

Abstract

The influence of particle-size distribution on the stress transfer mechanisms occurring in bimodal granular materials was investigated in this study. Efficient stress transfer is achieved when all particles within an assembly contribute to the resistance of applied loads. Both physical and numerical testing methods were employed including consolidated-undrained triaxial testing and numerical modeling using the discrete element method (DEM). Materials investigated included ideal spheres of stainless steel, polypropylene, and natural materials consisting of sand and silty-clay. Identification of critical mixture proportions according to percolation theory was attempted by examining the macro- and micro-mechanical response of bimodal distributions that were dominated by one fraction or were approaching the percolation threshold. Research results were inconclusive in validating the original hypothesis when comparing the numerical results to laboratory experiments. However, a relationship between coordination number and assembly stiffness was observed. Factors contributing to increased connectivity can also contribute to increased stiffness and shear strength.

Contents

Abstract ii

Figures and Tables v

Preface vii

List of Symbols/Terms viii

Unit Conversion Factors ix

1 Introduction 1

1.1 Research objective 2
1.2 Research approach 2
1.3 Organization of report 3

2 Background 4

2.1 Particulate materials 4
2.2 Macro/micro-scale interaction 5
2.3 Laboratory methods 6
2.4 Numerical methods 7
2.5 Particle-size distribution 8
2.6 Percolation threshold 9

3 Discrete Element Method 11

3.1 DEM in geomechanics research 12
3.2 Governing equations 19
3.2.1 Calculation cycle *21*
3.2.2 Velocity verlet algorithm *23*
3.2.3 Contact detection *24*
3.2.4 Parameter selection *25*
3.2.5 Critical time-step *25*
3.3 Horner, Peters, and Carrillo model 26
3.3.1 Model development *26*
3.3.2 Elements of the DEM model *27*
3.3.3 Spherical particles *28*
3.3.4 Facets *28*
3.3.5 Lines *29*
3.3.6 Rigid objects *29*
3.4 Parametric study 30
3.4.1 Effect of particle stiffness *31*
3.4.2 Effect of surface friction *32*
3.4.3 Effect of rolling resistance *34*

4 Experimental Validations 36
4.1 Testing program 36
4.2 Idealized particles 36
4.2.1 Consolidated-undrained triaxial testing 37
4.2.2 Testing results 41
4.3 Naturally occurring particles 47
4.3.1 Summary of testing presented by Peters and Berney 48
4.3.2 Testing results 48

5 Numerical Simulation of Bimodal Systems 51
5.1 Testing program 51
5.1.1 Specimen generation 51
5.1.2 Consolidation of particles 53
5.1.3 Simulation of triaxial testing 55
5.2 Testing results 56
5.2.1 Macroscale mechanical properties 57
5.2.2 Microscale mechanical properties 64

6 Analysis and Discussion 70
6.1 Macroscopic behavior 70
6.2 Microscopic behavior 71
6.2.1 Distribution of stresses 72
6.2.2 Coordination number 74

7 Summary and Conclusions 78

References 81

Report Documentation Page

Figures and Tables

Figures

Figure 1. Influence of particle proportioning on stress transfer mechanisms. 10
Figure 2. DEM of tined plow moving through particle system with colorization based on stress intensity (Horner et.al. 2001). 16
Figure 3. Linear-elastic particle contact model. 20
Figure 4. Illustration of a discrete element facet 29
Figure 5. Illustration of discrete element line element. 29
Figure 6. Illustration of a rigid object (plow) rendered in the discrete element model 30
Figure 7. Effect of particle stiffness on stress-strain behavior. 32
Figure 8. Effect of particle surface friction on stress-strain behavior. 33
Figure 9. Effect of particle rolling resistance on stress-strain behavior. 35
Figure 10. Particles examined in study: stainless steel (left) and polypropylene (right). 37
Figure 11. MTS triaxial compression testing apparatus. 38
Figure 12. Specimen preparation procedure: (a) lining mold with membrane, (b) prepared mold, (c) removing split mold, (d) specimen ready for testing. 40
Figure 13. Stress-strain behavior of uniform 0.1875-in. spheres. 43
Figure 14. Stress-strain behavior of stainless steel spheres at 15 psi. 45
Figure 15. Stress-strain behavior of stainless steel spheres at 50 psi. 46
Figure 16. Stress-strain behavior of polypropylene/ stainless steel spheres at 15 psi 46
Figure 17. Stress-strain behavior of polypropylene/ stainless steel spheres at 50 psi. 47
Figure 18. Stress-strain behavior of sand and silty-clay blends at 15 psi used in Peters and Berney (2010) study. 49
Figure 19. Stress-strain behavior of sand and silty-clay blends at 50 psi used in Peters and Berney (2010) study. 49
Figure 20. Stress-strain behavior of sand and silty-clay calibration curves. 50
Figure 21. Consolidated specimen of uniform spheres. 54
Figure 22. Stress-strain behavior of physical (solid) and model (dashed) uniform spheres. 59
Figure 23. Stress-strain behavior physical (solid) and model (dashed) sand/silty-clay materials from Peters and Berney (2010) study. 60
Figure 24. Stress-strain behavior of simulated stainless steel spheres at 15 psi. 60
Figure 25. Stress-strain behavior of simulated stainless steel spheres at 50 psi 61
Figure 26. Stress-strain behavior of simulated polypropylene/ stainless steel spheres at 15 psi. 61
Figure 27. Stress-strain behavior of simulated polypropylene/ stainless steel spheres at 50 psi 62

Figure 28. Stress-strain behavior of simulated sand/ silty-clay spheres at 15 psi 62
Figure 29. Stress-strain behavior of simulated sand/ silty-clay spheres at 50 psi. 63
Figure 30. Schematic of contact force components.....65
Figure 31. Shear stress distribution for polypropylene/stainless steel specimens at 15 psi (left) and 50 psi (right) confining pressure. 66
Figure 32. Shear stress distribution for stainless steel specimens at 15 psi (left) and 50 psi (right) confining pressure.....66
Figure 33. Shear stress distribution for sand/silty clay specimens at 15 psi (left) and 50 psi (right) confining pressure.....67
Figure 34. Stress porosity of stainless steel specimens at 15 psi (left) and 50 psi (right) confining pressure.....73
Figure 35. Stress porosity of polypropylene/stainless steel specimens at 15 psi (left) and 50 psi (right) confining pressure.....73
Figure 36. Stress porosity of sand/silty clay specimens at 15 psi (left) and 50 psi (right) confining pressure.....73
Figure 37. Influence of coordination number on shear strength of specimens sheared at 15-psi confining pressure. 77
Figure 38. Influence of coordination number on shear strength of specimens sheared at 50-psi confining pressure. 77

Tables

Table 1. Summary of select geomechanics works employing DEM. 13
Table 2. Average volumetric properties of stainless steel blends. 39
Table 3. Average volumetric properties of polypropylene/ stainless steel blends.....40
Table 4. Target number of spheres for consolidated laboratory specimen. 44
Table 5. Sphere distribution for numerical model consolidated specimen. 52
Table 6. Particle properties for materials simulated in DEM model. 53
Table 7. Volumetric properties of numerical model stainless steel blends. 54
Table 8. Volumetric properties of numerical model polypropylene/ stainless steel blends. 55
Table 9. Volumetric properties of numerical model sand/silty-clay blends. 55
Table 10. Calibrated particle properties for materials simulated in DEM model.....58
Table 11. Coordination number for stainless steel specimens. 68
Table 12. Coordination number for polypropylene/ stainless steel specimens.....68
Table 13. Coordination number for sand/silty clay specimens. 68
Table 14. Change in coordination number during shear of stainless steel specimens. 76
Table 15. Change in coordination number during shear of polypropylene/stainless steel specimens. 76
Table 16. Change in coordination number during shear of sand/silty clay specimens. 76

Preface

This study, entitled “Development of Ultra Compact Soil Science,” under project number 329090, was conducted by researchers at the U.S. Army Engineer Research and Development Center, Vicksburg, MS and sponsored by Headquarters, U.S. Army Corps of Engineers, Washington D.C. The program manager for this project was Dr. Ernest S. Berney IV.

The work was performed by the Airfields and Pavements Branch (APB) of the Engineering Sciences and Mobility Division (ESMD), U.S. Army Engineer Research and Development Center, Geotechnical and Structures Laboratory (ERDC-GSL) and the Instrumentation and Electronics Division (IE), Information and Technology Laboratory (ITL). At the time of publication, Timothy W. Rushing was Chief, APB; Dr. Gordon W. McMahon was Chief, ESMD; and Nicholas Boone was the Technical Director for Military Engineering. The Deputy Director of ERDC-GSL was Dr. William P. Grogan and the Director was Bartley P. Durst.

COL Bryan S. Green was the Commander of ERDC, and Dr. Jeffery P. Holland was the Director.

List of Symbols/Terms

2-D	two-dimensional space
3-D	three-dimensional space
DEM	discrete element method
EPS	expanded polystyrene
FCC	face-centered cubic
FEM	finite element method
F_f	frictional force
gm	gram
in.	inch
K	spring stiffness factor
ksi	kips per square inch
lbf	pounds force
mm	millimeter
No.	number
φ	angle of internal friction
psi	pounds per square inch
USCS	Unified Soil Classification System

Unit Conversion Factors

Multiply	By	To Obtain
cubic feet	0.02831685	cubic meters
cubic inches	1.6387064 E-05	cubic meters
feet	0.3048	meters
inches	0.0254	meters
microns	1.0 E-06	meters
mils	0.0254	millimeters
pounds (force)	4.448222	newtons
pounds (force) per foot	14.59390	newtons per meter
pounds (force) per square foot	47.88026	pascals
pounds (force) per square inch	6.894757	kilopascals
pounds (mass)	0.45359237	kilograms
pounds (mass) per cubic foot	16.01846	kilograms per cubic meter
pounds (mass) per square foot	4.882428	kilograms per square meter
pounds (mass) per square yard	0.542492	kilograms per square meter

1 Introduction

The design and evaluation of engineered granular media requires an understanding of the magnitude and distribution of stresses induced from application specific loading. Granular or particulate media includes soils, powders, agricultural grains, and industrial materials. The stress state of a granular assembly can be used to explain and predict engineering behavior. The response of particulate systems to externally applied loads is typically explained using constitutive theories, such as the critical state theory for soils, based on laboratory studies of macro-scale behavior. These methods rely upon measurements of boundary conditions to estimate the stresses within the specimen due to the difficulty of collecting internal measurements. Constitutive methods also require treating the particulate system as homogeneous, elastic, and isotropic. Most particulate systems, in particular soils, deviate from these idealizations often resulting in stress calculation errors ranging from 25 to 30 percent (Das 2010). Accurate prediction of the mechanical response of particulate systems requires an understanding of the stress transmission mechanisms within an assembly of particles without the constraints imposed by idealized constitutive theory based methods.

A number of researchers have begun examining the engineering response of particle systems using discrete numerical methods. Numerical models provide data on the particle-level mechanics, such as displacement, rotation, and inter- and intra-particle forces, which cannot be obtained through traditional laboratory instrumentation. Finite, particle based methods yield results more consistent with laboratory observations as compared to continuum methods (Armstrong and Dunlap 1966). Mathematical models such as the discrete element method (DEM) allow for simulation of traditional laboratory testing methods while also providing data on the micro- or particle-level mechanics driving the system. The DEM is an explicit numerical approach in which the interaction of particles is monitored contact by contact and the motion is monitored particle by particle (Cundall and Strack 1979). Data from the DEM can be used to investigate the micro-level physics, which control the observable, macro-mechanical performance of the material. This research seeks to use a DEM model to investigate stress transfer mechanisms by quantifying the influence of particle-size distribution on engineering performance. The principal

advantage of using numerical simulations is that all inter-particle data can be extracted from the assembly under investigation. Additionally, the influence of micromechanical properties can be more readily determined as compared to physical experiments (Bathurst and Rothenburg 1988).

1.1 Research objective

The transmission of stresses between particles is based upon a complex relationship determined by the particle-size distribution, loading history, fabric (assembly configuration), and particle characteristics (stiffness, shape, roughness etc.). Efficient stress transfer occurs when all of the particles in a consolidated assembly participate in resisting applied loads. The objective of this research is to investigate the influence of particle-size distribution on the stress transfer mechanisms occurring in binary particle systems. Many gap-graded materials commonly used in engineering can be approximated using binary systems (Peters and Berney 2010). This effort seeks to describe the engineering behavior of binary blends of particles by examining the micro- and macro-mechanical response of the systems to loading using both physical and numerical experiments.

1.2 Research approach

The objective of this research will be accomplished by examining the micro-mechanical data obtained from a DEM model to quantify the influence of particle-size distribution on macro-scale engineering performance. The DEM model developed by Cundall and Strack (1979) as implemented by Horner et.al (2001) will be used to simulate the triaxial compression testing of consolidated cubical specimens of particles. Systems of consolidated spheres in rhombic packing configurations will be generated using identical methods to eliminate the influence of other factors contributing to stress transfer mechanisms. The DEM model will provide data on the inter- and intra-particle forces, allowing for examination of the distribution of stresses and connectivity evolution amongst individual particles and between the discrete size fractions.

Additionally, the macro-mechanical properties of representative physical specimens will be determined by laboratory triaxial compression testing conducted in accordance with ASTM International standard test method D4767, *Standard test method for consolidated undrained triaxial compression test for cohesive soils* (ASTM 2004). The triaxial test is the most commonly used test for determining the constitutive response of

geotechnical materials. Although recent technical advancements in data collection have allowed measurement of some internal response within a triaxial test specimen including the evolution of localizations, some data are unattainable through physical testing including inter-particle forces (Cui et. al 2007).

The distribution of particles within discrete size fractions will be varied to define the influence of gradation on macro-mechanical properties. Both ideal spherical and naturally occurring particles will be examined in this investigation. Ideal particles will consist of discrete binary blends of stainless steel and polypropylene spheres. The particle-size distribution of many important engineering applications of granular materials can be approximated as binary mixtures including asphalt pavement, retaining structures, and dam and levee layers (Peters and Berney 2010). Idealizing soil grains as spherical particles departs from reality however; the idealization is sustainable when it provides useful information about material response (Bardet 1998). Naturally occurring particles will be investigated using data provided in Peters and Berney (2010). The authors used bi-modal grain-size distributions of sand and silty-clay particles to examine the theory of percolation. Future research is intended to consider real world particles represented by sand and silty-clay grain fractions.

1.3 Organization of report

Chapter 1 presents an introduction to the research topic. Chapter 2 of this document provides essential supporting background information used in development of the problem statement. The DEM numerical model is presented in Chapter 3 including the key features, history of development, and calibration parameters. Chapter 4 presents the details of the numerical simulations run as part of this investigation, and Chapter 5 presents the details of the laboratory testing. Chapter 6 presents analysis of results and relevant discussion. A summary of the conducted research and key conclusions resulting from the investigation is presented in Chapter 7. Finally, a list of referenced documents is presented.

2 Background

Any investigation of the behavior of granular materials in engineering applications requires knowledge of the stress and strain distributions occurring in the material (Oda and Iwashita 1999). Traditional methods for determining stresses (i.e., Boussinesq's equation for soils) require treating the particulate system as an idealized homogeneous, elastic, and isotropic system (Das 2010). Most particulate systems, in particular soils, deviate from these idealizations often resulting in calculation errors of 25 to 30 percent (Das 2010). The assumed stresses in a particulate system under a given loading configuration are the primary drivers in the design and evaluation of engineering systems.

Micromechanics explains the relationship between externally applied stresses and strains and internal forces and displacements (Sitharam et al. 2002). The micromechanics of granular media is a topic of interest for a number of technical fields including civil engineering, chemistry, metallurgy, pharmacy, and electrical engineering. Relationships between stress and strain can be examined phenomenologically or structurally. The traditional phenomenological approach relates measured mechanical properties to observed behavior and is analogous with constitutive theory based methods. A structural approach examines the mechanical behavior based upon the interactions of fundamental constitutive units. Finite methods are representative of the structural approach. Feda (1982) comments that the structural approach is required to understand the physical fundamentals of the mechanical behavior of particulate materials.

2.1 Particulate materials

Particulate material refers to objects ranging in size from boulders in a rock fill dam to submicron sized alloy powders in metallic components. In principle, these materials are very different, but the mechanical behavior due to the granular nature is, in fact, very similar. The wide range of objects that is regarded as particulate material exhibits similar behavior when tested under similar conditions, despite differences in size, shape, and composition. More important than the size of particles, the distribution of grain sizes greatly influences granular behavior (Hitcher 1998). Granular media are a subset of particulate materials that are visible to the naked eye.

The heterogeneous characteristics and configuration of grains are important mechanical features. Macroscopic behavior is determined by the arrangement and interaction of discrete grains (Oda and Iwashita 1999). Fabric describes the geometry of particle packing or microstructure (Bathurst and Rothenburg 1988). The fabric of granular materials provides insight on quantitative relationships between fabric and properties, mechanics of strength mobilization, nature of peak and residual strength, stress-strain behavior, and the effects of different sampling methods (Kuo and Frost 1997).

Particulate materials are composed of mutually contacting solid particles that exhibit shear induced volume change and sensitivity to hydrostatic stress. The behavior of particulate materials is controlled by the composition and dynamics of the composing particles. Particulate materials behave in a number of different modes including deforming as a solid, flowing as a fluid, or moving independently as individual particles. The multiple exhibited behavior modes are due to three-phase (solid, liquid, gas) composition, discontinuous arrangement, and heterogeneous nature (Oda and Iwashita 1999). The structural units of a particulate material are in mutual contact, which restricts the motion of each individual structural unit (Hitcher 1998). The degree of motion restriction is controlled by the magnitude of the applied stress. Subjected to small mean stresses granular materials flow like liquids; however, when subject to high stresses the materials can support large loadings (Hitcher 1998). Extremely complex continuum models are required to account for all of these different modes and requiring sophisticated model calibration techniques.

2.2 Macro/micro-scale interaction

The micromechanical behavior of particulate systems is commonly described using macro-scale measures of stress and strain. Historically, constitutive equations have been developed to describe the behavior of granular materials. With respect to soils, determination of the stress state under a particular loading configuration and proximity to the failure plane in the stress space are required for the design and evaluation of soil systems. The Mohr-Coulomb failure criteria are typically used to describe the critical combination of normal and shear stresses that define the failure plane for a given material. However, the internal friction angle used in the equation is not a material constant, but varies with void ratio, fabric, and stress state (Oda and Iwashita 1999). Applications that require knowledge of the stresses in a soil system include estimates of

compressibility, bearing capacity, stability, and lateral pressure applied to a retaining structure. The behavior of particulate materials, and in particular soils, is complex, and the development of a universally accepted model has yet to occur (Jiang and Yu 2006). The development of a universal model is obstructed by complex behaviors observed in granular materials including induced anisotropy, phase transformation, and non-homogeneity (Sitharam et. al 2002). The mechanics associated with large-scale soil deformation are poorly understood and traditional models are not applicable (Horner et. al 2001).

The macroscale properties of an assembly of particles including coefficient of contact friction, void ratio, particle shape, and size distribution are often used to describe observed mechanical behavior. The measurement of mechanical properties is more difficult and costly than the measurement of descriptive properties of particulate materials (Feda 1982). However, the underlying micromechanics are the true drivers of the system. The distinguishing characteristic of particulate material is that deformations occur as a result of sliding and realignment of particles versus deformation of the units themselves. Therefore, observed macro-scale deformation is a result of sliding and rolling at particle contact points. When observed at the microscale, the interaction of particles is simple with explicit material constants (Oda and Iwashita 1999). Particles transmit forces through a finite number of active critical contacts with neighboring particles (Christoffersen et. al 1981). The number and strength of contacts determine the strength and rigidity of a particulate material. Particles interact according to contact force/inter-particle compliance relationships at the contacts. Despite the apparent simplicity of the system, the behavior is quite complex at the microscopic level (Bathurst and Rothenburg 1988).

2.3 Laboratory methods

The shear strength of a soil mass determines the resistance to failure and sliding along the failure plane. Determination of strength parameters is often accomplished through direct shear or triaxial compression testing. The direct shear test is a simple and economical method for determining the strength parameters of soils. However, this method has a number of shortcomings including reliability of results and the non-uniform distribution of stresses (Das 2010). The triaxial shear test is widely used in both research and conventional applications. This method is regarded as highly reliable, although the equipment is costly and testing is time consuming relative to the direct shear test (Das 2010). Methods for

conducting triaxial testing include consolidated-drained (CD), consolidated-undrained (CU), and unconsolidated-undrained (UU) testing. Consolidated-drained testing is often used to determine the long-term stability of soil embankments. The CU test is used to examine the stability of consolidated structures undergoing rapid loading. Unconsolidated-undrained testing is used to evaluate the end-of-construction stability of saturated cohesive soils.

2.4 Numerical methods

The primary advantage of numerical techniques versus physical experiments is the generation of abundant information on particle displacements, contact forces, and other physical quantities. Numerical tests can be used to supplement real tests investigating the mechanical behavior of granular materials (Oda and Iwashita, 1999).

Continuum theory formulates engineering problems as mathematical boundary value problems. A major assumption of continuum theory is that material behavior observed in small laboratory tests can be extrapolated to large masses in the field. Hitcher (1998) comments that the Mohr-Coulomb criterion is merely an approximation of intermediate stress. Continuum approaches encounter issues due to instability and limitations in the constitutive equations. Continuum models employ a number of materials constants, some with no clear physical meaning (Oda and Iwashita 1999). Continuum mechanics may not be sufficient to express the overall mechanical properties of granular materials (Oda and Iwashita 1999).

Discrete modeling can be used to develop a fundamental understanding of material behavior that can aid in the development of physics based constitutive models. Discrete element approaches provide more realistic models of granular material behavior (Oda and Iwashita 1999). The primary limitation in applying discrete modeling techniques to soil mechanics is the number of particles required to simulate problems of engineering significance. A cubic centimeter of clay contains roughly 5×10^{12} particles while the most powerful computing platforms running in parallel can effectively handle around 10^7 particles. Limited computational ability has been overcome in previous studies by approximating the behavior of a volume of granular material using a single spherical element (Horner et. al 2001).

Bardet (1998) identifies eight discrete numerical techniques including distinct element, modal, momentum-exchange, multibody dynamics, structural mechanics, mean field, and energy minimization methods in addition to discontinuous deformation analysis. The original DEM, the distinct element method, was originally developed by Cundall (1974) and with minor modifications, is still the predominate DEM used today. The distinct element method is based upon the finite difference formulation of the equations of motion. The governing equations for the distinct element method yield resultant forces and moments at the center of particles resulting from contact, body, inertia, and damping forces. Assumptions of the distinct element method include particles are rigid spherical bodies, contact points between particles occur over an infinitesimally small area, particles can overlap slightly at contacts, the magnitude of the contact force is determined by the overlap magnitude, and slip between particles occurs according to Mohr-Coulomb law (Oda and Iwashita 1999). DEM requires relatively few calibration parameters and gives realistic results; a constitutive equation requires many (>15) parameters and only approximates behavior under a limited range of stress paths.

2.5 Particle-size distribution

The behavior of a granular material is strongly influenced by the grain size distribution of the composing particles (Evans et al. 2009). Armstrong and Dunlap (1966) comment that grain size distribution plays a significant role in particle interlocking and therefore, will have a definite effect on the stress-strain behavior. The primary effort in the design of granular material based technologies is the mixture design process. Successful mixture design is based on choosing proportions of coarse and fine materials to optimize desired mechanical properties (Peters and Berney 2010). The influence of grain size distribution applies to all particulate materials regardless of size. Additionally, it has been observed that the size ratio of particles dictates the packing density, not the absolute size (McGeary 1961).

Vallejo (2001) conducted laboratory and theoretical analyses to determine the influence of grain size distribution on developed porosity in bimodal blends of spherical glass beads. The author hypothesized that the properties and proportions of the composing binary blend of particles determine the macro-scale observable behavior. The beads consisted of 5.0- and 0.4-mm smooth glass with a specific gravity of 2.55. Laboratory testing consisted of uniaxial compression and direct shear testing at three different stress levels.

Findings of the Vallejo study included the fine material in bimodal mixtures reduces point to point contacts between coarse particles, preventing rotation and reorientation, to stabilize the assembly. Either the fine or coarse material, depending on the relative concentrations, controls the shear strength of bimodal distributions. A blend with greater than 70 percent coarse material behaves as a uniformly coarse material. Blends with less than 40 percent coarse material behave as a uniformly fine material. Blends between 70 and 40 percent coarse material exhibit transitional behavior dominated by contributions from both the fine and coarse material. The change in behavior observed at the previous limits is explained by the porosity of the different proportions. Particle angularity, surface roughness, and size distribution also influence the porosity of granular materials. Eliminating angularity and surface roughness through the use of smooth spherical particles allows for analysis based on size distribution alone. The minimum porosity condition is reached when the voids in the coarse matrix are completely filled with fine material. Binary mixtures can be classified as coarse grain supported, transitional coarse-fine grain supported, and fine grain supported structures depending on the coarse material concentration. Shear strength of the binary mixtures mirrored the relationship observed for porosity where maximum shear strength was observed at the same relative concentrations as minimum porosity (Vallejo 2001).

Deng and Xiao (2010) investigated and modeled the stress-strain characteristics of mixtures of expanded polystyrene (EPS) beads blended with sand at varying ratios of EPS content. Laboratory testing consisted of consolidated-drained triaxial compression testing. The EPS-sand mixtures were blended and compacted into 1.5-in. by 3.1-in. specimen. Specimens created with varying EPS content were tested in triaxial compression at four different confining pressures. The researchers observed a shift in the dominant shearing mechanism from dilative with well-defined peak strength to fully contractive with no indicated peak, as the EPS bead content was increased.

2.6 Percolation threshold

The percolation threshold in particulate materials references the critical proportioning of materials that allows for a transition in mass material behavior. The characteristics of a particulate mass are generally dictated by the properties of the most abundant material. The critical proportioning that causes the behavior of the blend to be dominated by one, versus the

other proportion, are determined by the properties of the composing materials (Peters and Berney 2010). The existence of the percolation threshold derives from percolation theory, which describes behavior associated with connectivity. The percolation threshold is characterized by dramatic changes in system behavior resulting from small changes in constituent composition fractions (Peters and Berney 2010). Thornton (2000) theorized sudden drops in coordination number may also indicate the percolation threshold, resulting in a transition in mechanical behavior.

Complimentary to the percolation threshold is the development and evolution of force chains. With respect to a binary granular material with both coarse and fine components, once the percolation threshold is reached, sufficient connectivity exists within the coarse fraction for the formation of force chains. Force chains develop in the large fraction as the proportion becomes significant enough for forces to be transmitted exclusively through the large fraction of the medium. Figure 1 illustrates a bimodal blend with behavior dominated by fine proportion (A), increasing the connectivity of the coarse proportion (B), and sufficient coarse proportion for the formation of force chains and shift in dominant proportion (C). When the percolation threshold of materials such as sand and silty-clay blends as studied by Peters and Berney (2010) is reached, erratic and even unstable behavior was observed.

Figure 1. Influence of particle proportioning on stress transfer mechanisms.

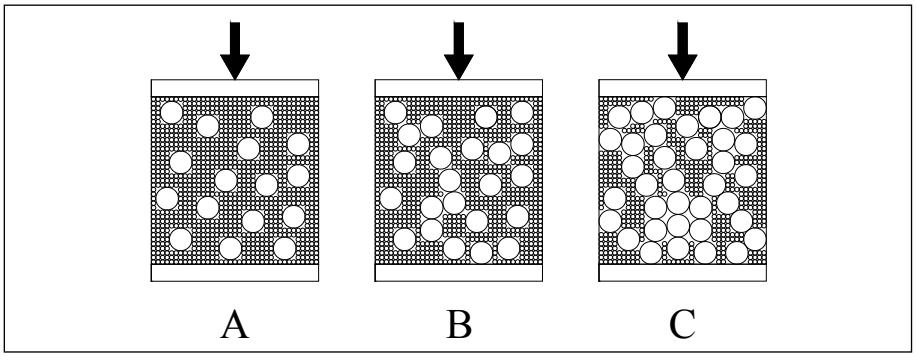

3 Discrete Element Method

Inter-particle forces greatly influence granular material behavior, but it is virtually impossible to measure inter-particle forces in real granular materials (Peters and Berney 2010). Due to the difficulty in directly measuring, the forces are typically estimated from the boundary forces measured in physical testing. The discrete element method (DEM) is a numerical method for simulating the behavior of particle-based systems by integrating the equations of motion for each body in an assemblage of particles (Cundall and Strack 1979). The method treats each particle within the assemblage as a rigid, discrete body. Binary contact laws define the forces and motions that occur in the system. Contact forces and displacements are calculated for equilibrium conditions where incremental changes in contact force are determined by incremental displacements at the particle contact. Newton's second law of motion is integrated to obtain the net forces and moments acting on each particle. This approach deviates from other numerical methods such as finite elements in that the observed macro-scale behavior is a result of the definition of particle interactions versus a definition of the assemblage.

DEM refers to a number of numerical computational methods for modeling granular materials. Bardet (1998) describes eight and O'Sullivan (2002) documented 15 different discrete numerical methods. Advantages of DEM include the ability to model a wide variety of complex granular flow and rock mechanics applications while generating detailed data on the micro-mechanics occurring at the particle scale not obtainable using physical experiments. The primary disadvantage of DEM is that the method is computationally intensive and thus, scaled models of actual systems incorporating thousands of particles versus billions must be used in order to obtain results in a reasonable time period. Cundall (1974) developed the numerical method known as the distinct element method to describe the mechanical behavior of granular materials. The distinct element method is an explicit scheme in which the behavior of a system of particles is determined by interactions at shared contacts.

The distinct element method is designed for applications where large displacements are of interest. The primary assumption of the distinct element method is that macro-scale deformations are a result of the rolling

and sliding of spherical particles and not deformation of the particles themselves. The assumption of non-deformable particles is valid in low-stress situations where rotation and sliding are the primary mechanisms of movement. However, in conditions where the magnitude of particle loading is very high inducing particle deformation of a similar magnitude to the deformation in the system, the distinct element method models will not be valid and another approach, such as the finite element method, should be investigated (Cundall 1974). Cundall and Strack (1979) observed that precise modeling of particle deformation was not required to accurately simulate mechanical behavior. An additional assumption of the method is that particles interact at the point of contact and forces are adjusted until a state of equilibrium is reached. Cundall (1974) comments that the assumption that particle interactions can be adequately modeled by two localized forces seems more valid than the conventional assumption of a continuous uniform stress because real particles typically only touch at a few asperities regardless of surface smoothness.

3.1 DEM in geomechanics research

The DEM has been successfully used by a number of researchers to provide insight on the micromechanics of granular systems while accurately simulating macro-scale behavior. A summary of select works documenting the utilization of DEM in geomechanics research is presented in Table 1. The DEM was originally developed as a two-dimensional (2-D) numerical method for predicting deformations in rock structures (Cundall 1974). Other researchers including Cundall and Strack (1979), Jiang and Yu (2006), and Evans et al. (2009) have applied 2-D DEM for deeper understanding of the underlying micromechanics occurring in granular materials.

Cundall and Strack (1979) validated the performance of discrete numerical models by reproducing historical results from a photoelastic analysis of an assemblage of discs. The photoelastic analysis consisted of loading two horizontal and two vertical beams that formed the boundaries of an assemblage of discs. The bounding beams were loaded and allowed to freely rotate. The motion of the discs was recorded to construct force vector plots. The physical experiment was simulated using the distinct element method to obtain a qualitative assessment of the effectiveness of discrete numerical models for modeling the behavior of particulate systems. The authors observed good correspondence between the physical test and numerical simulation and concluded the distinct element method is effective for modeling the fundamental behavior of granular assemblies (Cundall and Strack 1979).

Table 1. Summary of select geomechanics works employing DEM.

Author(s)		Title	Keywords
P.A.	Cundall	A Discrete Numerical Model for Granular Assemblies	2-D DEM, discs, axisemmetric compression, photoelastic analysis
O.D.L.	Strack		
M.	Jiang	Application of Discrete Element Method to Geomechanics	2-D DEM, discs, grain size distribution, noncoaxality, effective stress, bonding, penetration,
H.S.	Yu		
T. Matthew	Evans	Grain Size Distribution Effects in 2D Discrete Numerical Experiments	2-D DEM, discs, biaxial compression, grain size distribution
Hamed	Mojarrad		
Charles	Cunningham		
Akhtar A.	Tayebali		
C.	Thornton	Numerical Simulations of Deviatoric Shear Deformation of Granular Media	3-D DEM, spherical particles, axisemmetric compression, packing density, contact force, coordination number, anisotropy
S. Joseph	Anthony	Evolution of Force Distribution in Three-Dimensional Granular Media	3-D DEM, spherical particles, cubical specimen, axisemmetric compression, packing density, interface energy
David A.	Horner	Large Scale Discrete Element Modeling of Vehicle-Soil Interaction	3-D DEM, spherical particles, finite elements, high performance computing, parallelization, particle interaction, mass deformation
John F.	Peters		
Alex R.	Carrillo		
L.	Cui	Exploring the Macro- and Micro-Scale Response of an Idealized Granular Material in the Direct Shear Apparatus	3-D DEM, spherical particles, direct shear, steel spheres
C.	O'Sullivan		
Thallak G.	Sitharam	Micromechanical Modeling of Monotonic Drained and Undrained Shear Behavior of Granular Media using Three-Dimensional DEM	3-D DEM, spherical particles, triaxial compression, stress path, packing density, coordination number, anisotropy
S.V.	Dinesh		
N.	Shimizu		
Catherine	O'Sullivan	Examination of the Response of Regularly Packed Specimens of Spherical Particles Using Physical Tests and Discrete Element Simulations	3-D DEM, spherical particles, triaxial compression, uniform and non-uniform size distribution, steel spheres
Jonathan D.	Bray		
Michael	Riemer		
Catherine	O'Sullivan	Experimental Validation of Particle-Based Discrete Element Methods	2-D/3-D DEM, circular rods, spherical particles, non-uniform size distribution, biaxial compression, triaxial compression, direct shear
Jonathan D.	Bray		
Liang	Cui		
L.	Cui	An Analysis of the Triaxial Apparatus using a Mixed Boundary Three-Dimensional Discrete Element Model	3-D DEM, spherical particles, triaxial compression, steel spheres, contact force, fabric
C.	O'Sullivan		
S.	O'Neill		
Tang-Tat	Ng	Discrete Element Simulations of the Critical State of a Granular Material	3-D DEM, ellipsoidal particles, cubical specimen, triaxial compression
N.	Belheine	Numerical Simulation of Drained Triaxial Test using 3D Discrete Element Modeling	3-D DEM, spherical particles, triaxial compression, Labenne sand
J.P.	Plassiard		
F.V.	Donze		
F.	Darve		
A..	Seridi		

Jiang and Yu (2006) present applications of DEM to geomechanics. Topics covered are based on the authors' previous research and include noncoaxiality of granular materials, effective stress in unsaturated soils, bonding effect in natural soils, and penetration mechanisms in granular ground. The DEM model used in the study was a modified version of the code presented by Cundall and Strack (1979). The authors observed good agreement between DEM simulations and laboratory simple shear testing. The authors used the DEM as a virtual laboratory to gather data not possible in physical testing. The DEM was observed to be an effective tool for examining the noncoaxiality of granular materials, effective stress in unsaturated granular materials, bonding effect in natural soils, and complex boundary value problems in geotechnical engineering.

Evans et al. (2009) investigated the influence of grain size distribution on the stress-strain-strength behavior of 2-D systems of particles. A DEM numerical model was used to simulate biaxial compression testing on four distinct grain size distributions including coarse, medium, and fine well-graded and uniformly graded distributions. Elliptical particles with an aspect ratio of 1.5 to 1.0 were used in the model and were composed by bonding pairs of identical spheres. The authors concluded that DEM is capable of modeling the response of well-graded assemblies in addition to the more simple gradations typically used.

The accurate simulation of physical systems requires accurate representation of the modeled media in three-dimensional (3-D). A number of researchers have extended successful 2-D simulations of granular material behavior into 3-D. Thornton (2000), Antony (2000), Horner et al. (2001), and Cui and O'Sullivan (2006) have all used 3-D DEM to investigate the behavior of granular media.

Thornton (2000) investigated the use of DEM models to simulate 3-D polydisperse systems of elastic spheres in axisymmetric compression, radial deviatoric loading, constant deviatoric strain, and multi-axial plane strain testing. The specimens consisted of five discrete sized particle distributions. The author observed the stress-strain-dilation response of simulations was similar to laboratory observations of axisymmetric compression. Thornton concluded, "Realistic 3-D stress-strain dilation behavior can be generated by discrete element simulations."

Antony (2000) investigated the evolution of contact normal force distribution in monodisperse particulate systems using DEM simulations. The DEM model included a submerged particle system containing 5,000 uniform spheres in a cubical periodic cell undergoing axisymmetric compression. Variables included noncohesive particles, low interface energy, packing density, and stiffness. The transmission of forces during slow shearing was analyzed. The author found DEM to be an effective tool for investigating the micromechanics of particulate systems.

Horner et. al (2001) present the promise and associated concerns when parallelized DEM modeling is applied to discontinuous, large deformation soil-vehicle interaction problems. The authors modeled the deformation in a soil mass resulting from the interaction with a tined plow using a 3-D DEM consisting of 10,000,000 particles optimized for use on a parallelized high performance computing platform. The authors comment on the value of modeling vehicle design alternatives in a virtual environment and on the difficulty of using continuum based methods. The particulate nature of the DEM allows for modeling discontinuous large deformations encountered in such problems. The authors applied a joint DEM finite element method (FEM) model to accurately simulate the phenomenon observed in field-testing. The authors concluded that DEM captures the particulate phenomenology of soils and avoids the programming complexity of traditional constitutive methods. The researchers also observed a remarkable level of detail in DEM simulations of large-scale deformation also observed in physical testing (Figure 2).

Figure 2. DEM of tined plow moving through particle system with colorization based on stress intensity (Horner et.al. 2001).

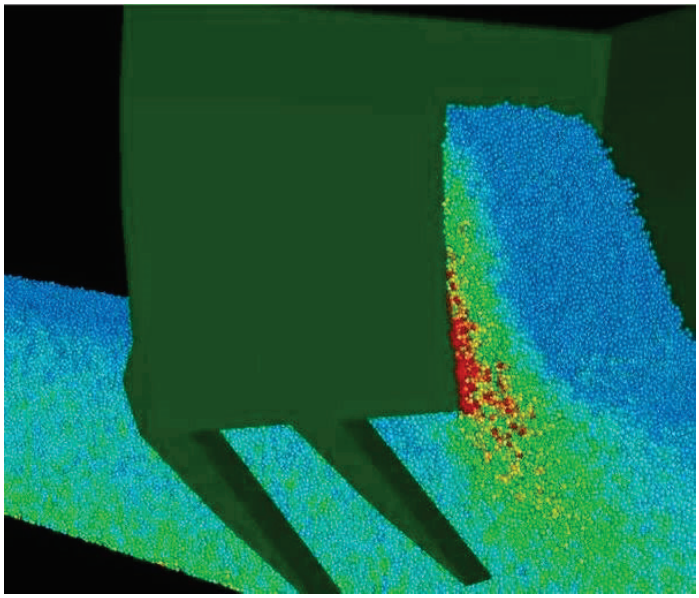

Cui and O'Sullivan (2006) examined the similarities and differences in micro- and macro-performance of idealized granular assemblies composed of uniform steel spheres. Laboratory testing included direct shear tests on steel sphere assemblies with varying normal load at a fixed velocity. DEM simulations of the direct shear tests were attempted using material properties determined in the laboratory. The macro-performance of the physical and numerical testing were compared, and micro-mechanical performance measures including distribution of force, displacements, rotations, specimen fabric, and variation in volumetric shear strain determined using the DEM model. The DEM model was found to effectively simulate the direct shear test. The model did under-predict the peak shearing resistance angle; however, the authors hypothesized that the differences may be caused by non-constant inter-particle friction in physical models (increasing with strain). The DEM confirmed theories about inhomogeneities in stress, strain, and rotation in the direct shear test.

Triaxial compression testing is the primary method for determining strength and deformation behavior in geomechanics. Most commonly accepted constitutive theories for soil behavior have been developed using extensive triaxial testing. A number of researchers including Sitharamet. al (2002), O'Sullivan et. al (2004), O'Sullivan et. al (2006), Cui et. al (2007), Ng (2009), and Belheine et al. (2009) have used 3-D DEM simulations of triaxial testing to develop an understanding of the underlying micromechanics of soils subjected to external loading.

Sitharam et. al (2002) investigated the evolution of induced anisotropy during drained and undrained triaxial tests on loose and dense assemblies of spheres using a DEM model. Simulations were conducted on assemblies of 1,000 spherical particles with lognormal particle-size distributions representing Unified Soil Classification System (USCS) GP and SP soils. Simulation of the triaxial testing of cubical specimens was accomplished with a focus on the evolution of microscopic features of the granular assembly. The simulation of triaxial undrained tests was accomplished with DEM by maintaining a constant volume of the specimen during shear. The authors comment on the difficulty in modeling the complex behavior of soils including induced anisotropy, phase-transformation, low-confinement behavior, and non-homogeneity using traditional continuum mechanics approaches. In granular materials, such as soils that are dominated by particulate behavior, it is advantageous to treat the medium as an assemblage of particles rather than a continuum. The authors conclude that DEM models are valuable in geomechanics because they provide complete quantitative data on all microscopic features of an assembly of particles.

O'Sullivan et. al (2004) investigated the response of spherical, idealized granular assemblies in both physical and numerical experiments. Physical testing included plain strain and triaxial compression tests. The numerical experiments employed a DEM model to simulate the physical testing by matching the properties of the spheres observed in physical testing to include friction angle, fabric (void ratio, coordination number), and packing configuration. The DEM simulations were able to accurately capture the peak response of the tested materials. However, the post-peak behavior was difficult to model and was determined to be a function of discrepancies in specimen fabric. The researchers concluded that the DEM was effective for monitoring both changes in coordination number and strength, with the strength of the specimen decreasing with decreasing coordination number.

O'Sullivan et. al (2006) set out to quantitatively demonstrate that DEM models could accurately simulate the response of granular materials. A series of three DEM validation tests were undertaken in the investigation. The first study examined the 2-D response of uniform and almost uniform hexagonally packed rods. The biaxial compression of 2-D hexagonally packed rods was examined in the laboratory and modeled using DEM. The second study was an extension of the first looking at the 3-D response of

uniform spheres in face-centered-cubic (FCC) and rhombic packing arrangements in triaxial and plane strain compression. The culminating study examined the response of randomly packed spheres in the direct shear test. The DEM models were found to be able to accurately replicate the response of granular materials in standard laboratory tests while providing insight into the particle-scale interactions driving the observed macro-scale response. The DEM was found to satisfactorily simulate laboratory response up to the peak strength. However, post-peak response could not be captured without modification of model parameters. The authors concluded DEM modeling is a valuable tool for engineers examining the micro-scale mechanics driving the response of granular materials.

Cui et. al (2007) studied the micro-scale response of systems of steel spheres in triaxial testing using both physical testing and DEM modeling. Mixed boundary 3-D DEM code was used in the study to accurately simulate the latex membrane and imposed confining pressure used in the physical triaxial test. Testing was performed on assemblies of uniform and tri-modal discrete sphere sizes in face-centered-cubic (FCC) packing arrangement. Coupling DEM simulations and triaxial tests on ideal spheres allowed for accurate replication of the material, facilitating quantitative validation of the model. The authors commented that the quality of the validation would have been compromised by the use of more complex materials such as real soils. It was recommended to validate DEM models using simple materials prior to incorporating more complex “real” materials to ensure accuracy and appropriateness of the model.

Ng (2009) uses a series of DEM simulations to examine the critical state of three cubical assemblies of ellipsoids. The critical state was reached by simulating axial compression, lateral extension, and constant mean-stress compression tests at varying confining pressures. The critical state line in void ratio, mean stress, and deviator stress space was explored. The numerical experiments challenged conventional theory on the critical state line. Curvature was observed in the critical state line in simulations of rigid materials, suggesting that the curvature in physical experiments is not solely due to particle breakage. The author found DEM to be an effective tool for examining the micromechanics of soil structures.

Belheine et al. (2009) investigated the effectiveness of a DEM model in reproducing macro-scale behavior of a granular material. A DEM model

was used to simulate drained triaxial testing of Labenne sand. Ten thousand spherical particles were used in the 3-D DEM model. The authors found the discontinuous nature of granular materials to induce unique behaviors such as anisotropy, micro-fracture, and local instability. The DEM model used in the study reproduced the non-linear stress-strain behavior of Labenne sand. The DEM was also able to accurately produce the Mohr-Coulomb criterion for the modeled material. The researchers found the numerical and experimental results to be in good agreement.

3.2 Governing equations

The DEM is an iterative, cyclic calculation numerical model. The inter-particle contact forces are calculated for each particle using the relative velocities and the employed force-displacement laws. The behavior at the contact is critical to effective modeling because the interaction of particles is characteristic to the material of interest (Hitcher 1998). The force and moment sums are used to compute the linear and rotational accelerations of each particle, which are numerically integrated to yield velocity, and integrated again to give displacement according to Newton's second law of motion. Contact checks are then performed prior to initiation of the next calculation cycle. Although the DEM system is dynamic, it can be approximated as static, if the loading rates at the boundaries are small enough that the inertial forces are small compared to the contact forces.

Forces in the system arise from deformations occurring between particles, assumed to occur at the shared contacts. The contact interaction of the particles can be modeled using a set of springs, dashpots, and a frictional slider as shown in Figure 3. Elastic force/displacement laws are used in the DEM and are incremental, where a change in displacement produces a change in force, which is added to the existing force (Cundall 1974). For every time-step, the incremental normal and shear displacements for a given contact are evaluated from the incremental rotational displacement.

Figure 3. Linear-elastic particle contact model.

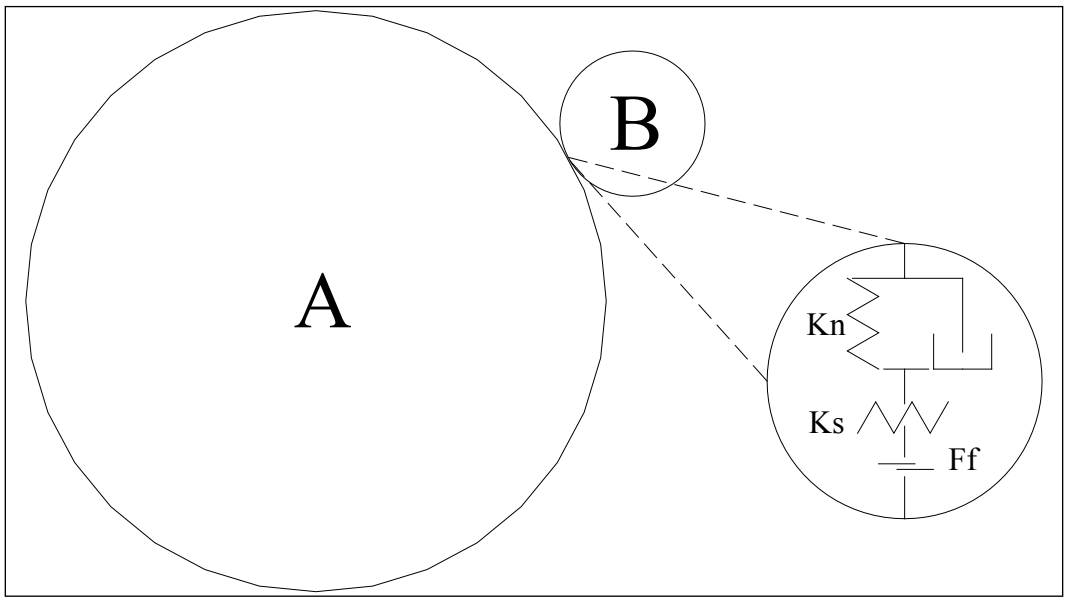

The normal and shear forces are calculated using the existing and incremental forces according to the force/displacement equations. The incremental contact forces are resolved in x and y forces and moments and added to the existing x and y forces and moments. Linear elasticity is sufficient to describe the behavior of grains except were high stresses result in plastic deformation or rupture of the grains (Hitcher 1998). Elastic spheres interact in a non-linear manner, but a linear spring model is useful for verification of theoretical concepts (Bathurst and Rothenburg 1988).

To prevent excessive energy buildup, a spring-dashpot system is employed to model the conversion of kinetic to thermal energy taking place at the contact points in a physical system. The inclusion of damping allows the assembly of particles to reach equilibrium. Damping is achieved mathematically by connecting viscous dashpots in parallel with the normal and shear stiffness at each contact (Cundall 1974). The particle material is elastic, but through the use of energy dissipating mechanisms at the contact, the overall behavior is inelastic (Sitharam et. al 2002). No explicit rotational damping is employed in the DEM. Cundall and Strack (1979) commented that damping does not influence the force equilibrium value but reduces the number of calculation cycles required to reach equilibrium. Damping is incorporated to allow a state of equilibrium to be reached in the model. However, the departure from equilibrium can also be minimized by reducing the loading rate (Cundall and Strack 1979).

3.2.1 Calculation cycle

The calculation cycle begins by determining the relative velocity and rotational rate of each particle in the assembly according to Equations 1 and 2, respectively.

$$m\frac{\partial \nu_i}{\partial t} = mgn_i^g + \sum_{i=1}^{N_c} f_i^c \tag{1}$$

where:

ν_i = velocity
t = time increment
m = mass
gn_i^g = acceleration due to gravity
N_c = number of contacts
f_i^c = force at the contact

$$I_m \rho \frac{\partial w_i}{\partial t} = \sum_{c=1}^{N_c} e_{ijk} f_i^c r_j^c + \sum_{c=1}^{N_c} m_i^c \tag{2}$$

where:

w_i = rotational rate
I_m = moment of inertia
ρ = unit weight
r_j^c = radius from the particle center to the point of contact
m_i^c = moment applied at the contact

A determination of particle contact is then conducted by evaluating each particle and its nearest neighbors. Two particles are in contact if the distance between the particle centers is less than the sum of the combined radius as shown in Equation 3.

$$d < R_A + R_B \tag{3}$$

where:

d = distance between the centers of particles A and B
R_A = radius of particle A

R_B = radius of particle B

For two particles in contact, the overlap or displacement at the contact is determined according to Equation 4.

$$\Delta_i^c = \nu_i^A - \nu_i^B + e_{ijk}\left(r_j^A w_k^A - r_j^B w_k^B\right) \tag{4}$$

where:

Δ_i^c = relative motion at the contact
ν_i^A = velocity of particle A
ν_i^B = velocity of particle B
r_j^A = radius from the center of particle A to the point of contact
w_k^A = rotational rate of particle A
r_j^B = radius from the center of particle B to the point of contact
w_k^B = rotational rate of particle B

The rotational difference between two particles in contact is determined as shown in Equation 5.

$$\Delta w_i^c = \Delta t\left(w_i^A - w_i^B\right) \tag{5}$$

where:

Δw_i^c = difference in rotation of particles A and B
Δt = change in time increment
w_i^A = rotational rate of particle A
w_i^B = rotational rate of particle B

The force-displacement laws are applied to determine the forces and moments acting on each particle as a result of interaction with another particle. The normal force, shear force, and moment at each contact are determined in accordance with Equations 6 through 8, respectively.

$$f^n = \begin{Bmatrix} K^n \Delta^n \\ E_r K^n \left(\Delta^o - \Delta^n\right), \Delta^n < \Delta^o \end{Bmatrix} \tag{6}$$

where:

f^n = normal component of the contact force
K^n = normal stiffness constant
Δ^n = normal component of the contact displacement
E_r = an energy dissipation factor
Δ^o = greatest magnitude of penetration in the history of the normal contact displacement

$$f_i^s = \begin{cases} K^s \Delta_i^s \\ f^n \tan\varphi n_i^s, \left| f_i^s \right| \geq f^n \tan\varphi \end{cases} \quad (7)$$

where:

f_i^s = shear component of the contact force
K^s = shear stiffness constant
Δ_i^s = shear component of the contact displacement
φ = a force friction parameter
n_i^s = shear force unit vector

$$m_i^c = \begin{cases} K^m \Delta w_i^c \\ f^n \tan\varphi_m n_i^m, \left| m_i^c \right| \geq f^n \tan\varphi_m \end{cases} \quad (8)$$

where:

m_i^c = moment at the contact
K^m = moment stiffness constant
n_i^m = moment unit vector

3.2.2 Velocity verlet algorithm

The velocity verlet algorithm is a numerical method for integrating Newton's second law of motion. The algorithm is a "leapfrog" approach that uses the current position, velocity, and acceleration to calculate the future state. The linear and rotational velocities are integrated to yield the future linear and rotational accelerations and applied as shown in Equations 9 and 10 for the future position and velocity and Equations 11 and 12 for the angle of rotation and angular velocity.

$$r_{n+1} = r_n + \Delta t v_n + \frac{1}{2}\Delta t^2 a_n \tag{9}$$

where:

r_n = the position of the particle at the nth time-step
υ_n = the velocity
a_n = the acceleration

$$v_{n+1} = v_n + \frac{1}{2}\Delta t\left(a_n + a_{n+1}\right) \tag{10}$$

$$\theta_{n+1} = \Delta t w_n + \frac{1}{2}\Delta t^2 \alpha_n \tag{11}$$

where:

θ_n = the angle of rotation of the particle at the nth time-step
w_n = the rotational rate
α_n = the angular acceleration

$$w_{n+1} = w_n + \frac{1}{2}\Delta t\left(\alpha_n + \alpha_{n+1}\right) \tag{12}$$

Once the position, velocity, and acceleration of each particle in the assembly for the next time increment have been determined, the calculation cycle is restarted.

3.2.3 Contact detection

Simplified DEM models achieve contact detection by comparing the distance between particles with every other particle in the assemblage. This procedure requires significant computational effort as the number of calculations increases N^2 as the total number of particles (N) increases. Most practical DEM models employ a nearest neighbor search procedure to define contact between particles. The nearest neighbor approach assigns each particle to a cell space based upon its Cartesian coordinates. Thus, when checking for contacts only the adjoining cells need be evaluated. This approach is very simple for uniformly sized particles; however, when a distribution of particle sizes is used, a bounding box cell search scheme is

employed. In this method the cell size is determined by the smallest particle size, and the bounding box is the collection of all the cells in which any portion of the particle crosses (Peters et al. 2010*). The contact detection is conducted only on the cells within the bounding box for each particle to ensure maximum computational performance.

3.2.4 Parameter selection

The material properties of a continuous solid cannot be used directly when selecting parameters for the DEM model. Armstrong and Dunlap (1966) propose the analogy that if a steel cylinder were machined into spheres, the mass of spheres would not exhibit the same modulus of elasticity or Poison's ratio as the original cylinder. The selection of material properties is accomplished such that the observed performance resembles physical observations. However, parameters should also be selected to minimize particle overlapping in relation to particle size, ensure stability of the system, and the values calculated in the program are in a range that can be handled with accuracy (Cundall and Strack 1979). Cundall and Strack (1979) observed that while other parameters can be adjusted in an effort to optimize the program, the inter-particle friction angle and the ratio of shear and normal stiffness should be selected based upon the physical properties of the material being modeled. O'Sullivan et. al (2004) emphasize the importance of using the physical characteristics of the material being modeled as parameters in DEM simulations.

3.2.5 Critical time-step

Failure in particulate systems is often prefaced by a number of particle realignments as the loads are redistributed. Cundall (1974) commented that the sequence and magnitude of the motions are important to the conditions precipitating final failure due to the high degree of non-linearity in a particulate system. Thus, the DEM incorporates an explicit numerical method, where the entire system of equations is solved with small increments of time, or time-steps. Use of the explicit method allows for tracking the path to failure, versus an implicit method, which is more efficient from a time perspective but may skip over some of the important effects.

* Peters, J. F., R. Kala, R. S. Maier, L. Walizer, J. Wibowo, and R. E. Wahl. 2010. *User guide for DEM development.*

The discrete element model relies upon explicit integration, which is only conditionally stable. The DEM is based upon the idea that a time increment so small can be selected in the explicit scheme so that during a single increment interactions caused by a given particle cannot propagate beyond the nearest neighbors (Cundall and Strack 1979). The time-step required for stability, or critical time-step, is a function of the mass and stiffness of the particles, with the most critical relationship as defined by the natural oscillating frequency (Cundall and Strack 1979). The DEM program used in this study selects a time-step 0.10 times the critical time-step, calculated according to Equation 13, and based on the smallest and stiffest particles in the system. The critical time-step limitation often requires compromises during the calibration of the model (Peters et al. 2010). To achieve acceptable run times the stiffness must be assigned low or the mass assigned high. Acceptable results have been achieved when applying either approach. Scaling particle mass does not affect stresses and strains as opposed to scaling particle stiffness. However, the velocities and accelerations are reduced in magnitude (Thornton 2000). Peters et al. (2010) recommend exercising caution when adjusting material properties to expedite run times, especially when examining dynamic problems where the fundamental frequency of the mass can be an issue.

$$\Delta t = 2\sqrt{\frac{m}{k}} \tag{13}$$

where:

Δt = the critical time-step
m = the particle mass
k = the particle stiffness

3.3 Horner, Peters, and Carrillo model

3.3.1 Model development

The Horner et. al (2001) model simulates the 3-D movement of spherical particles as they interact with one another and rigid solid objects defined by finite elements. The development of the model was driven by studies for modeling large-scale deformations in systems of particles. The original code was modified with an emphasis on micro-scale interactions that could be run on a standard PC in serial based code. The current code is

written in FORTRAN 95 and is intended for the micro-mechanical research of engineering materials.

The objective of Horner et. al (2001) was the development of a 3-D large-scale soil modeling system. The implementation of a discrete element method (DEM) model for the simulation of vehicle soil interaction was the focus of the effort. The developed model consisted of three sections to model the physics of soils to include calculation of boundary and global body forces, calculate forces between particles, and integrate equations of motion in accordance with Newton's second law. The original algorithm loops through the previously described actions on a particle by particle basis for the duration of the simulation. Horner's model has been optimized through code efficiencies and a new contact detection algorithm. A serial version of this optimized code is employed in this study. As of this study, due to the computational time requirements, only a few tens of thousands of particles can be simulated on a personal computing platform. One-to-one simulation of a triaxial compression specimen composed of sand would require approximately 200,000 particles. Simulation of field applications using the same sand would require well over 1 million particles.

The authors (Horner et. al 2001) investigated the use of coarsened particulate models where each particle in the simulation represents a large volume of particulate media. DEM was used to simulate the movement of a tined plow through a mass of sand. The authors determined that the location and width of the shear band as well as the motion of particles within the band could be accurately predicted with the DEM model.

3.3.2 Elements of the DEM model

The DEM model used in this study is composed of spherical particles and rigid objects. Other elements that are available in the model include non-spherical particles and membranes. The DEM model was developed to provide data on inter- and intra- particle forces and displacements of the particles. Therefore, the other objects are limited in the manner in which they interact. The particles can interact with both particles and other objects in the model; however, rigid objects and membrane can only interact with particles and themselves.

3.3.3 Spherical particles

Spherical particles are the primary elements of interest in the current study. Although non-spherical particles more accurately represent the shape of actual soils, spherical particles were selected to reduce the computation time for the model. The particles are defined by the location of the centroid, radius, and density of the particle. The state of the particle at any time increment is defined by the position, linear and rotational velocity, and cumulative force and moment. The cumulative forces and moments arise as each particle interacts with other particles and rigid bodies in the model. Additionally, the mass of the particle is assumed to be uniformly distributed so that the moment of inertia tensor is isotropic (Peters et al. 2010).

3.3.4 Facets

The interaction of particles with rigid objects in the model is defined through contact with facets. Facets are 3-D, oriented triangular surfaces used to define rigid objects (Figure 4). The facets are defined similarly to finite elements using connectivity tables to monitor the coordinates of each facet's vertices. A particle is considered to be in contact with a facet if the distance between the particle centroid and the facet face is less than the radius of the particle, and the potential contact point between the particle and facet lies within the boundaries of the facet. These contact criteria are insufficient at the edge or corner of a rigid object where the potential contact point can lie outside the boundary of the facet yet the particle and facet are in contact. Line elements are used in the model to account for occurrences where the particle is in contact with the edge or corner of an object.

Figure 4. Illustration of a discrete element facet.

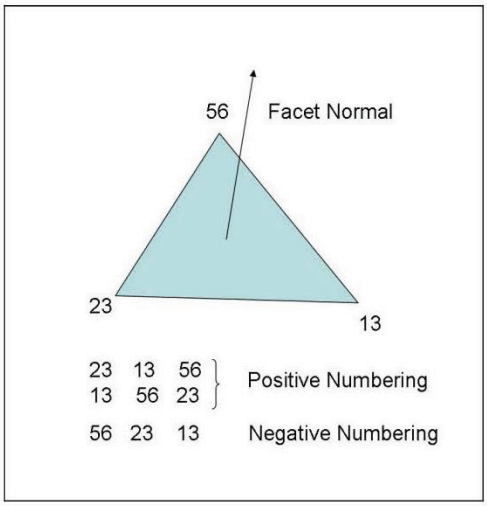

3.3.5 Lines

The line element is used to connect two facets at the edge or corner of an object (Figure 5). Line elements are defined similarly to facets except the connectivity only requires the two nodes defining the endpoints. The contact criteria for facet elements is insufficient at the edge or corner of an object where a particle can be in contact with a facet; however, the potential point of contact lies outside of the facet boundary. The line element is used to resolve the inherent ambiguity.

Figure 5. Illustration of discrete element line element.

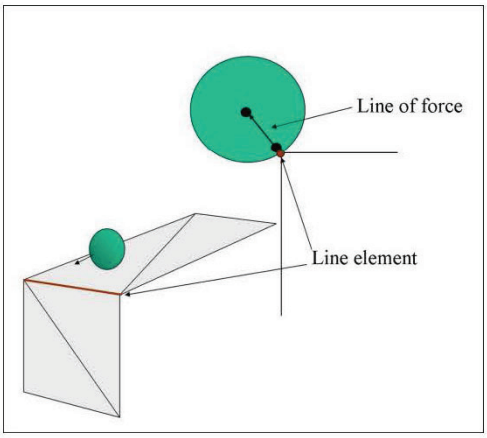

3.3.6 Rigid objects

Rigid objects are the principal means for imparting boundary conditions on a system of particles. The rigid object is defined by the collection of

facets and lines that make up the surface, the mass of the object, and the moment of inertia (Figure 2 and Figure 6). Rigid objects can move through three linear displacement and three rotational degrees of freedom. The movement of the rigid object can be controlled using either force (or moment) or velocity (displacement and rotation) variables. The movement of the rigid objects is tracked by updating the nodes of the composing facets and lines using a coordinate transformation consisting of translation and rotation about the center of mass (Peters et al. 2010). The forces and moments applied to the facets are accumulated at the center of mass for the six degrees of freedom. Unlike finite elements, the facet and lines are treated independently and therefore do not have to be connected.

Figure 6. Illustration of a rigid object (plow) rendered in the discrete element model.

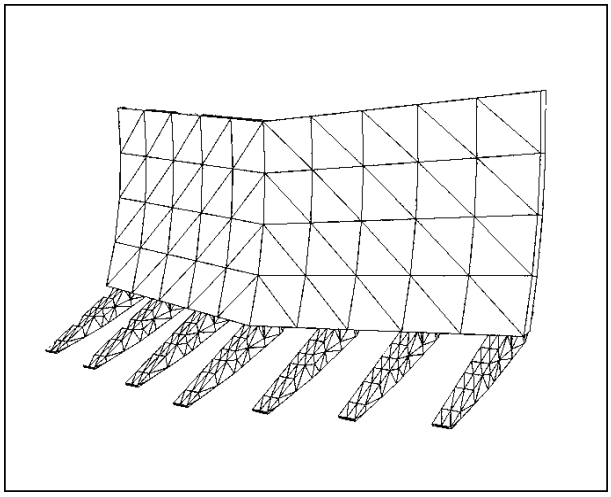

3.4 Parametric study

DEM models allow for simulation of particulate-based materials in a wide variety of engineering applications. The primary parameters that control the behavior of a system of compacted particles include: specific gravity, contact stiffness, surface friction, and rolling resistance. While specific gravity, contact stiffness, and surface friction are properties of the modeled media, rolling resistance is a calibration factor employed to account for the use of spherical particles in modeling non-spherical materials. When simulating triaxial compression testing, the axial force, confining pressure, and loading rate can be specified.

Prior to beginning the research effort outlined in Chapter 1, a parametric study was undertaken to gain familiarity with the influence of the primary material parameters on engineering behavior. The interaction of particles

is modeled using sets of springs, dashpots, and a frictional slider. An effort was made to accurately represent the materials of interest as recommended by O'Sullivan et. al (2004). Therefore, material properties representative of a USCS classified (SP) quartz sand were used during the parametric study to include a specific gravity of 2.65, normal and shear spring stiffness (K^n and K^s) of 5.0×10^6 psi, friction coefficient (u) of 0.50, and rolling resistance (R) of 50.0 to account for the use of spherical particles. Additionally, the triaxial testing was conducted under strain control with an initial deviator stress of 50 psi and a loading rate of 0.05 in./sec. The influence of particle stiffness, surface friction, and rolling resistance were investigated by varying each property within a finite range while all other parameters were held constant.

3.4.1 Effect of particle stiffness

The effect of particle stiffness on the engineering behavior of compacted cubical specimens subjected to triaxial compression was investigated using a serial version of the Horner, Peters, and Carrillo DEM model. The specimens consisted of approximately 7,000 uniform particles with a diameter of 0.80 in. and the properties of SP sand as previously described. The specimen generation process is discussed in detail in Chapter 5.

Particles interact in the DEM model in accordance with linear-elastic contact laws based upon Hooke's law rather than a Hertzian contact law typical in most DEM soil mechanics models. The particle stiffness is determined by the magnitude of the spring constant assigned in the normal (K^n) and shear (K^s) directions. For this research, the ratio of normal to shear stiffness was maintained at 1:1 and illustrates the stress-strain relationship on the particle matrix for this stiffness condition for K values ranging from 500,000 to 50,000,000 psi (shown in Figure 7). Cundall and Strack (1979) observed the ratio of normal and shear stiffness to have a significant influence on the behavior of a particulate system. The influence however, was reduced at low friction angles due to the early onset of slip. Belheine et al. (2009) also observed that elastic response is controlled by the ratio of shear to normal contact stiffness. The shear force is controlled exclusively by the normal force once slip has occurred in accordance with the Mohr-Coulomb criteria (Cundall and Strack 1979). Due to the use of spherical particles, it was hypothesized that the onset of slip would occur early in testing and the use of a 1:1 ratio was found to approximate that response effectively in the DEM.

The strength of the particulate system modeled using DEM was greatly influenced by the prescribed contact stiffness. Intuitively, as the stiffness is increased the peak stress also increases when the strain is held constant. In particular, an increase in stiffness results in a significant increase in shear stress. The mean stress measured during triaxial compression is also increased but to a lesser degree. In addition, an increase in stiffness results in greater dilative tendency as indicated by significant drops in calculated pore water pressure.

Figure 7. Effect of particle stiffness on stress-strain behavior.

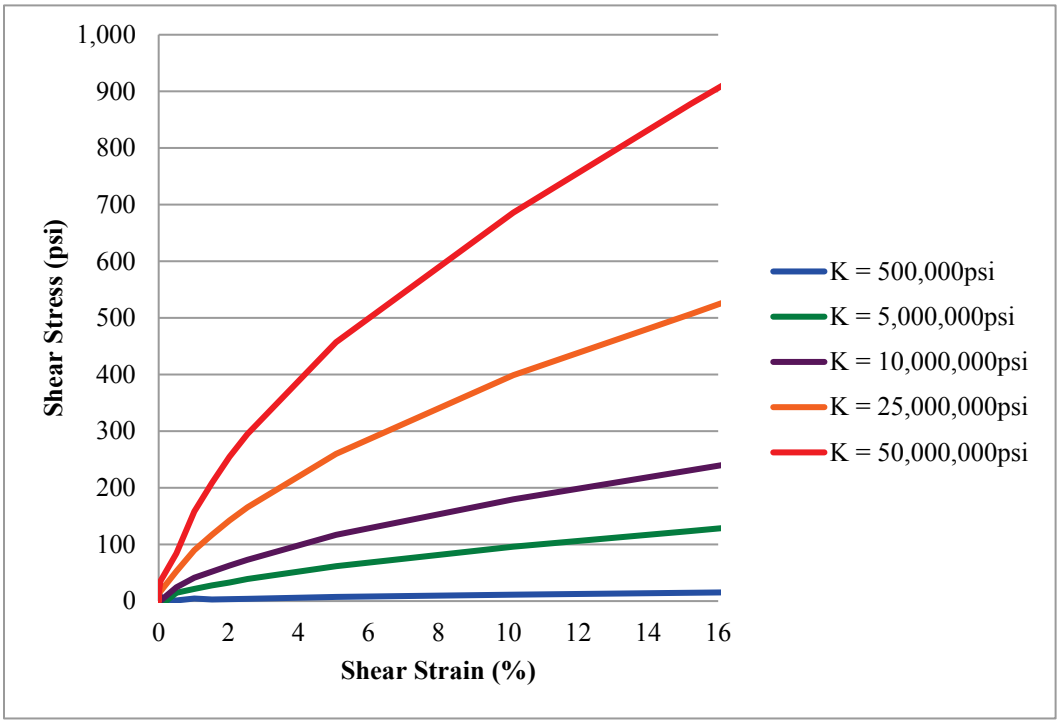

3.4.2 Effect of surface friction

Similar to particle stiffness, the influence of surface friction on the engineering behavior of particulate assemblies was investigated using the DEM model. The coefficient of friction (u) describes the force of friction between two contacting particles in accordance with the Mohr-Coulomb criterion ($u = \tan \varphi$). Particle stiffness and rotational resistance were held constant as the particle surface friction coefficient was varied from 0.1 to 5.0 as shown in Figure 8, noting that during initial loading the particle rearrangement caused shear stress-strain inconsistencies. Increasing inter-particle friction results in increased initial stiffness (Cui et. al 2007). Friction at the contact controls the macro-deformation and strength

behavior of granular materials (Oda and Iwashita 1999). Deformation depends strongly on local friction (Belheine et al. 2009). The friction activated at the contacts between structural units determines the shear strength of a particulate material. The mechanical behavior is closely related to the translational and rotational friction (Feda 1982). However, Cavarretta et. al (2010) found macro-scale performance to be more greatly influenced by particle shape than surface roughness.

Overall shearing resistance is increased with greater inter-particle friction. The application of pore pressures can be used to overcome inter-particle friction and force a particulate material into a fluid state (Feda 1982). At high stress levels, the influence of surface friction is reduced (Cavarretta et. al 2010). The magnitude of stress fluctuations is influenced by system size and particle roughness (Shearer and Schaeffer 1997).

Figure 8. Effect of particle surface friction on stress-strain behavior.

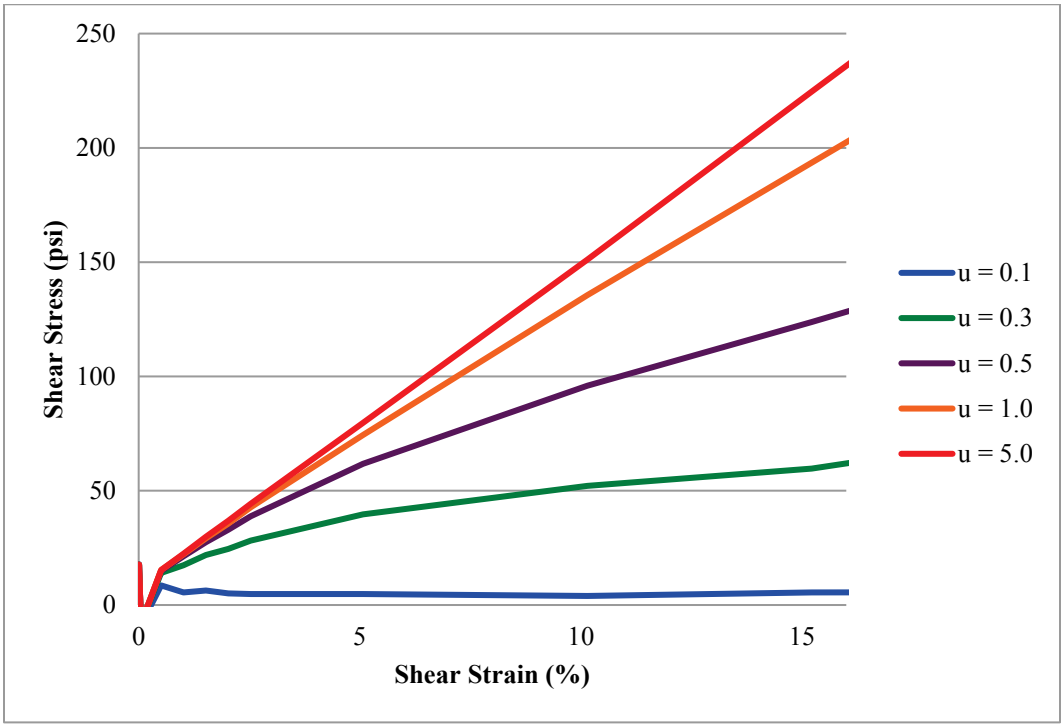

Figures 7 and 8 exhibit stress-strain behaviors of simulated specimens undergoing triaxial compression testing. The peak shear stress of the compacted system, and likewise the peak mean stress increased with increased inter-particle friction, *u*. However, the inter-particle friction is not proportional with bulk material properties. The influence of inter-particle friction is greater at lower bulk values; at higher bulk values, an

equal change in inter-particle friction has a reduced effect. At sufficiently low values of friction, the particle assembly was observed to rotate freely, similar to a ball bearing and the system reaches a steady state of consolidation.

3.4.3 Effect of rolling resistance

The influence of rolling resistance was also investigated using the DEM model. Rolling resistance can be applied when modeling irregularly shaped granular materials using spherical particles. Resistance to rolling is not a material property. Instead, it is a calibration parameter used in modeling of spheres to ascertain the engineering response in a pseudo non-spherical manner. The rolling resistance coefficient (R) is a scaling factor that increases the rotational and torsional moments to account for the resistance that would be provided by the geometry of irregular shaped particles according to Equation 14.

$$m_i^c = m_i^c + (R \times \Delta t \times \Delta w_i^c) \tag{14}$$

"Using rolling resistance between spherical discrete elements is justified since real grains are generally not spherical and may exhibit a rough surface texture which can be covered with a thin film of weathered products." (Belheine et al. 2009). Rolling resistance has great influence on the contact behavior of the granular material. Rolling resistance does not affect the translational motion but does affect the angular motion (Belheine et al. 2009). Feda (1982) states that if contact stiffness is increased to prevent sliding and rotation, a particle assembly will lose freedom of motion and behave as a continuous solid which would create an unrealistic particulate model. Therefore, while particle stiffness and the surface friction coefficient were held constant, the rolling resistance factor was varied from 5.0 to 500.0 as shown in Figure 9.

Figure 9. Effect of particle rolling resistance on stress-strain behavior.

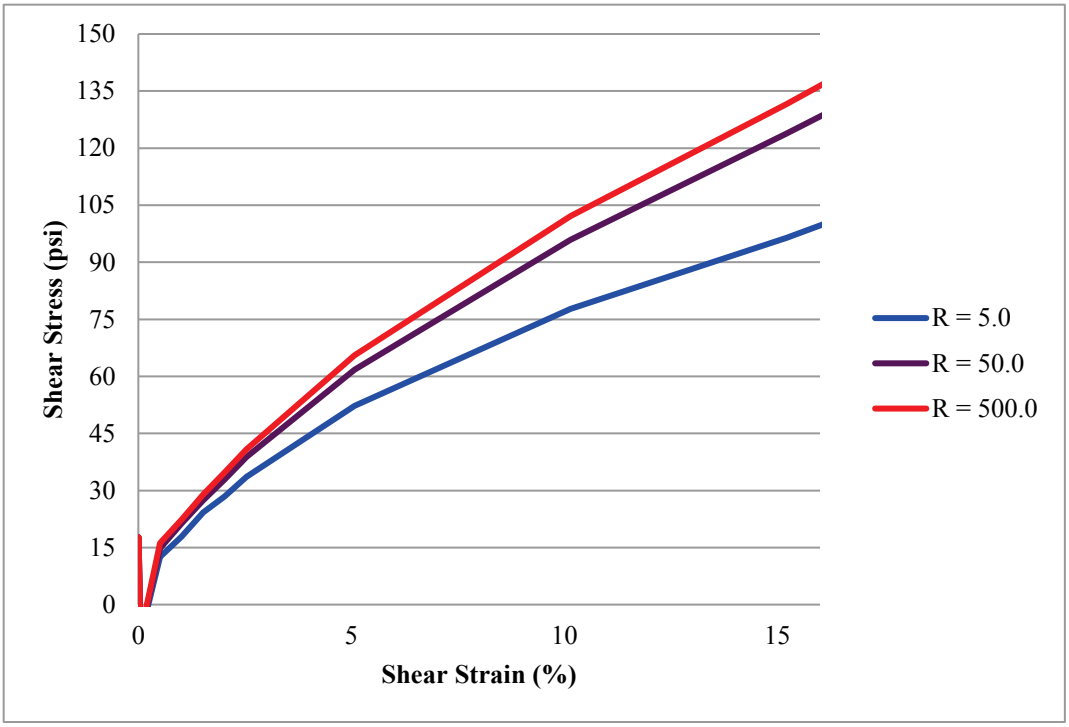

The influence of rolling resistance was examined using a simulated sand material undergoing triaxial compression testing. Increasing rolling resistance results in a minor increase in peak stress. In particular, the shear stress in the system is slightly increased with essentially no increase in mean stress. However, the greatest influence of increasing rolling resistance can be seen in the volumetric changes induced in the material undergoing shearing. Increasing rolling resistance increases contractency and decreases dilatancy potential. In Figure 9, at a rolling resistance of 5, the sand material exhibits a lower overall shear strength than at a value of 500. This increase in strength at a high rolling resistance supports the occurrence of increased dilatancy between particle contacts.

4 Experimental Validations

4.1 Testing program

The objectives of the physical testing regimen were to develop calibration curves for the DEM and to validate the mechanical performance of bimodal particle distributions subjected to simulated triaxial compression testing. Laboratory testing consisted of triaxial compression of consolidated particulate specimens in accordance with ASTM D 4767, *Standard test method for consolidated undrained triaxial compression test for cohesive soils* (ASTM 2004). The standard testing method is often used to determine the shear strength of soils in a variety of engineering applications to include embankment stability analysis, earth pressure calculations, and foundation design (ASTM 2004). Undrained testing was selected for the granular medium as pore pressure response allows measurement of volume response in a more comprehensive and finer resolution than vertical and horizontal strain measurements of the cylindrical sample. An effective stress path can be calculated from the CD DEM model to allow comparisons to the CU laboratory results. Initially, assemblies of uniform particle sizes were constructed and tested to produce data for calibration of the DEM model. Bimodal blends were then used to validate the behavior observed in the numerical simulations. Both stainless steel and polypropylene materials were used with sphere diameters of 0.75 in. and 0.1875 in. Peters and Berney (2010) used an identical testing approach to examine the behavior of bimodal blends of sand and silty-clay. The central theme of that work was the identification of a critical mixture ratio identified using percolation theory.

4.2 Idealized particles

The particles used in the laboratory investigation consisted of 0.75-in.- and 0.1875-in.-diam spheres composed of stainless steel or polypropylene as shown in Figure 10. All the spheres used in this study were obtained from Bal-tec. Bal-tec is a division of Micro Surface Engineering Incorporated, located in Los Angeles, California, specializing in the manufacture of precision balls and bearings. The stainless steel balls are type 440C stainless steel that consists primarily of chromium and ferrite. Type 440C stainless steel is used widely in anti-friction applications where high hardness and corrosion resistance are required. The material has Rockwell Hardness of

58 and a density of 0.277 lb/in.^{3}. Polypropylene is a thermoplastic polymer used in a number of engineering and industrial applications. The material is extremely corrosion resistant but is flexible and resists fatigue. The polypropylene material used in the manufacture of the spheres has an average Rockwell Hardness of 90 and a density of 0.033 lb/in.^{3}. The manufacturing quality of the spheres is indicated by the respective grades. The stainless steel spheres were a grade 25, indicating maximum deviation from target diameter and sphericity of 2.5 x 10^{-5} in. The polypropylene spheres were a grade 3 with maximum deviation of 3 x 10^{-6} in.

Figure 10. Particles examined in study: stainless steel (left) and polypropylene (right).

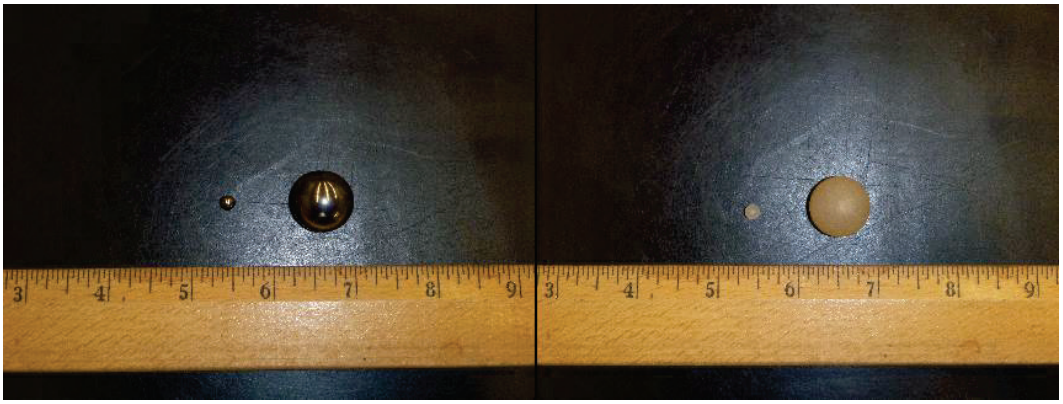

4.2.1 Consolidated-undrained triaxial testing

Consolidated-undrained triaxial compression testing conducted in accordance with ASTM D 4767 (ASTM 2004) provides data on the strength and stress-strain relationship of a cylindrical particulate specimen. Specimens were saturated, consolidated isotropically, and sheared using a constant rate of compression without drainage. Determination of total and effective stresses is possible through measurement of axial load, axial deformation, and pore-water pressure.

4.2.1.1 Testing apparatus

The testing apparatus used in this study was custom manufactured by MTS Systems Corporation for the U.S. Army Engineer Research and Development Center (ERDC). The apparatus consisted of an axial loading frame, hydraulic supply, electronic controller, load cell, linear variable differential transformer (LVDT) and pore-water pressure transducer, all conforming to the standards provided in ASTM D 4767 (ASTM 2004) and presented in Figure 11.

Figure 11. MTS triaxial compression testing apparatus.

The triaxial compression chamber was modified from its initial manufacture to accommodate the instrumentation required for the experiments. The hydraulically driven loading frame consists of a MTS Model 312 load frame with 55-kip maximum capacity, Model 510 hydraulic supply and Model 293 hydraulic manifold capable of supplying 3,000 psi of pressure, and Flex Test GT digital controller. The frame can be either load or displacement controlled. Displacement control was used with a loading rate of 0.05 in./min for this investigation. The BLH Electronics Model U3G1 electronic load cell has a maximum capacity of 5,000 lbf and provides 1 x 10^{-3} lbf precision. The RDP Group Model LDC1000A LVDT measures the axial deformation of the specimen with a maximum vertical displacement of approximately 3.0 in. and provides 1 x 10^{-7}-in. precision. The pore-water pressure is measured using a Sensotec

K2 electronic pressure transducer with an optimal operating range of 5 to 350 psi, providing 1 x 10^{-6}-psi precision. The triaxial compression chamber is a sealed reinforced chamber capable of withstanding pressures up to 250 psi. The cap and base are made of aluminum, the mounting pedestal is made of brass, and the cylindrical walls are made of reinforced Lucite. The base and pedestal provide ports for the introduction and removal of gases and liquids to the chamber, specimen, or both.

4.2.1.2 Specimen preparation

The specimens constructed for this investigation were cylindrical with a 4-in.-diam and a target 8-in. height. Due to the irregular packing of the spheres, some deviation in the specimen height (±0.25 in.) was observed. Specimen preparation can have a dramatic effect on laboratory performance (Kuo and Frost 1997). To reduce potential for introduction of error into the testing program, the procedure provided in ASTM D 4767 (ASTM 2004) was adhered to for the construction of each tested specimen. The average volumetric properties for the stainless steel and polypropylene/ stainless steel blends prepared for this investigation are presented in Tables 2 and Table 3, respectively.

The number of particles required to fill the 4-in. by 8-in. target specimen where calculated based upon volume, blended together (only for bimodal blends), and compacted in a split cylindrical mold in six layers using a tamping rod. The split cylinder was lined with a 0.025-in.-thick neoprene membrane prior to addition of the spheres. Once the target height was achieved, a vacuum was applied to the specimen, now encased in the neoprene membrane, and the split cylinder mold removed. The specimen preparation procedure is presented pictorially in Figure 12.

Table 2. Average volumetric properties of stainless steel blends.

Particle Fraction % (coarse to fine)	15 psi eff. confining stress			50 psi eff. confining stress		
	Mass (gm)	Height (in.)	Void Ratio	Mass (gm)	Height (in.)	Void Ratio
0-100	8,300	7.93	0.60	8,300	7.95	0.60
40-60	9,060	7.82	0.43	9,060	7.90	0.43
45-55	9,230	7.98	0.43	9,231	8.04	0.43
48-52	9,174	7.90	0.43	9,174	8.00	0.43
50-50	9,228	7.88	0.42	9,228	7.99	0.42
52-48	9,281	7.87	0.41	9,281	7.99	0.41
60-40	9,244	7.78	0.40	9,244	7.88	0.40

Table 3. Average volumetric properties of polypropylene/ stainless steel blends.

Particle Fraction % (coarse to fine)	15 psi eff. confining stress			50 psi eff. confining stress		
	Mass (gm)	Height (in.)	Void Ratio	Mass (gm)	Height (in.)	Void Ratio
0-100	8,300	7.93	0.60	8,300	7.95	0.60
40-60	5,888	8.16	0.48	5,888	8.14	0.47
45-55	5,505	8.20	0.45	5,505	8.18	0.45
48-52	5,421	8.08	0.45	5,520	8.10	0.45
50-50	5,149	8.16	0.45	5,149	8.13	0.45
52-48	4,977	8.19	0.44	4,977	8.13	0.44
60-40	4,260	7.98	0.42	4,260	7.97	0.42

Figure 12. Specimen preparation procedure: (a) lining mold with membrane, (b) prepared mold, (c) removing split mold, (d) specimen ready for testing.

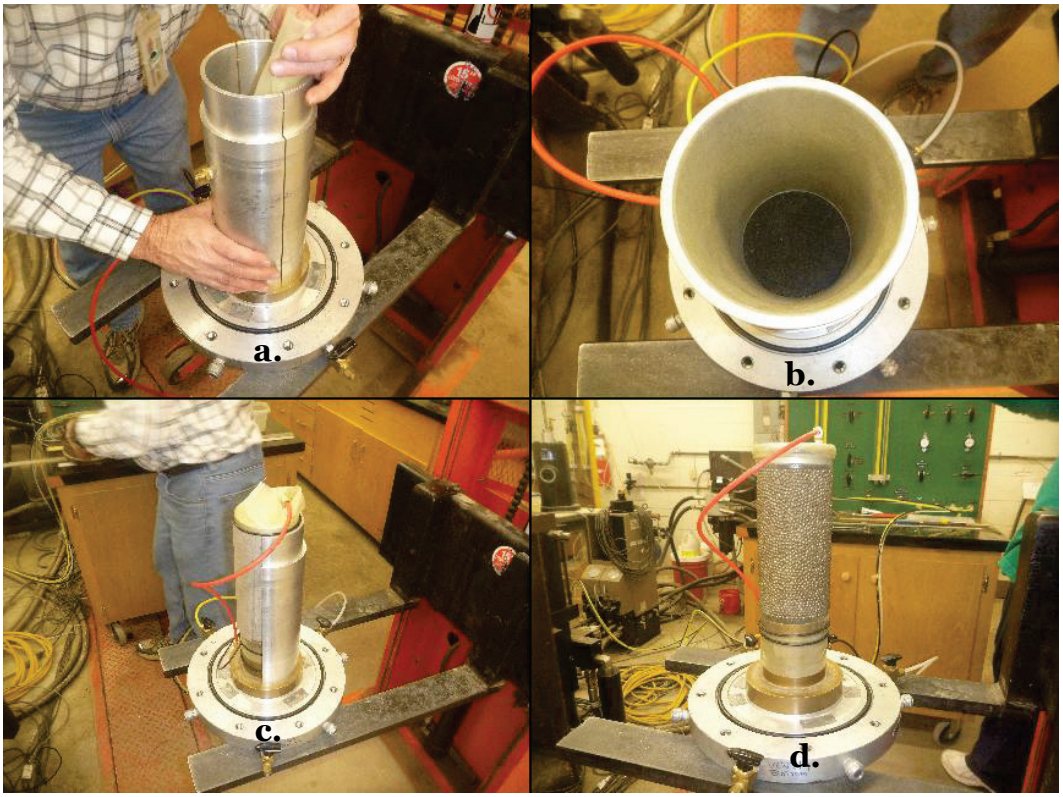

4.2.1.3 Testing procedure

Aluminum top and bottom caps were applied to the specimen and the assembly mounted on the pedestal within the triaxial compression chamber. Water and vacuum lines were connected to allow water to enter and exit the specimen and a vacuum to be applied to both the specimen and

the chamber. The chamber was then sealed and mounted within the loading apparatus. Air was used to apply the confining pressure in this investigation. The specimen was then saturated by allowing water to flow from the bottom cap, through the specimen, to the top cap. Once the specimen was nearly saturated, 70 psi of backpressure was applied to force any remaining air into solution and fill all voids with de-aired water.

A check of the B-value, the ratio of the change in pore-water pressure resulting from changes in confinement pressure, was then conducted to determine the responsiveness of the specimen. A B-value greater than or equal to 0.95 indicated the ability to begin testing; a value less than 0.95 indicated that additional back pressurization was required. Holding the backpressure constant and increasing the chamber pressure was used to achieve the target effective confining pressure. Confining pressures of 15 psi and 50 psi were used in this investigation. The effective confining pressure was held constant, the drainage valves closed, and an axial load was applied to the specimen to induce shear. The axial loading was displacement controlled at a rate of 0.05 in./min. Testing was discontinued when 10 percent axial strain or shear failure of the specimen was observed.

4.2.2 Testing results

Data were collected during triaxial compression testing at a sampling rate of 2.0 Hz and included time elapsed, axial load, axial displacement, chamber pressure, and backpressure. The data were used to calculate shear stress, effective mean stress, shear strain, and excess pore-water pressure using Equations 15 through 19, respectively.

$$\sigma_{shear} = \sigma_1 - \sigma_3 \tag{15}$$

where:

σ_{shear} = shear stress

σ_1 = vertical principal stress (axial load/specimen area)

σ_3 = chamber pressure

The change in cross-sectional area during shear was approximated using Equation 16.

$$A_{adjusted} = \frac{\pi d^2}{4(1-\epsilon_{axial})} \quad (16)$$

where:

$A_{adjusted}$ = cross-sectional area of the specimen resulting from increasing axial strain
d = specimen diameter
ε_{axial} = axial strain (change in height/initial height)

$$\varepsilon_{shear} = 1.5 * \varepsilon_{axial} \quad (17)$$

where ε_{shear} is the shear strain.

$$\Delta\mu = \mu - \mu_i \quad (18)$$

where:

$\Delta\mu$ = excess pore-water pressure
μ = backpressure at any time
μ_i = initial backpressure

$$\sigma'_{mean} = \frac{\sigma_1 + 2\sigma_3}{3} - \mu \quad (19)$$

where σ'_{mean} is the effective mean stress.

The initial set of experiments was conducted on uniform assemblies of 0.1875-in.-diam spheres. The testing was conducted on both the stainless steel and polypropylene materials at 15-psi and 50-psi confining pressure. The objective of these experiments was to develop characteristic curves for the materials used in the study and apply these curves for the calibration of the DEM material model. Two tests were run for each material type and confining stress level combination and the resulting shear stress, excess pore water pressure and effective mean stress for each combination were averaged together for each level of shear strain. The average stress-strain characteristic curves developed using the procedure previously described are presented in Figure 13.

Figure 13. Stress-strain behavior of uniform 0.1875-in. spheres.

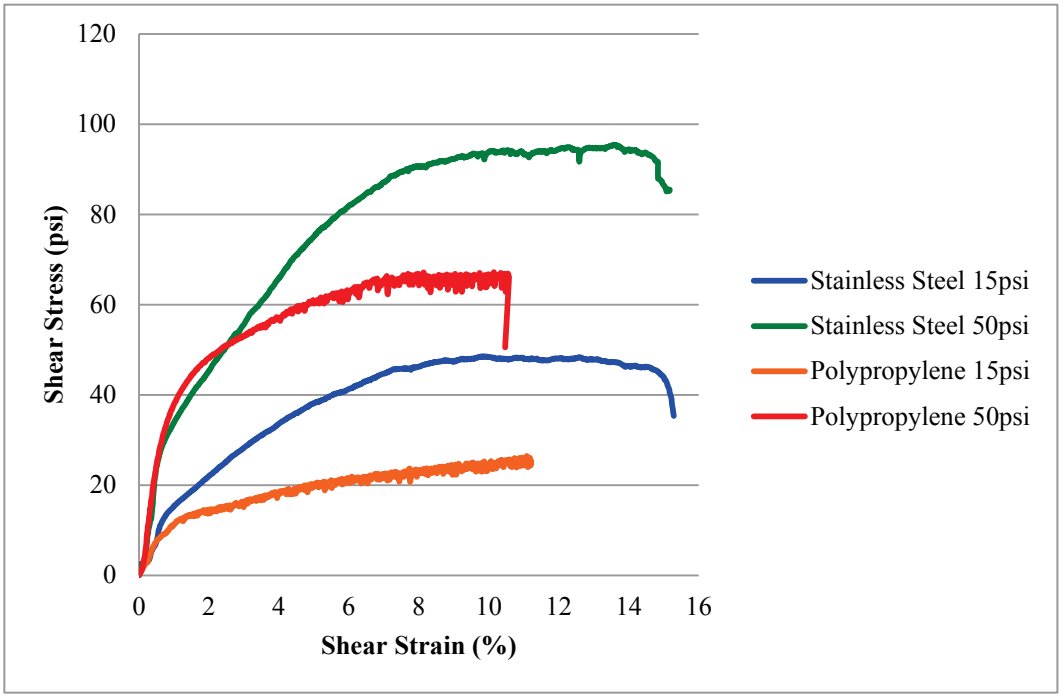

Once the characteristic curves were developed, blends of the stainless steel spheres were created and tested to examine the influence of particle-size distribution on engineering performance. The specimens were generated and tested as described in the "Consolidated-undrained triaxial testing" section. Initially, blends of 40 percent (by volume) 0.75-in.-diam spheres and 60 percent 0.1875-in.-diam spheres were examined at both 15-psi and 50-psi confining pressure. These blends were designated 40 to 60 percent (0.75 to 0.1875 in.). Two tests were run at each stress level and confining stress level combination and the resulting shear stress, excess pore water pressure and effective mean stress for each combination were averaged together for each level of shear strain.

This process was repeated for increasing proportions of 0.75-in. (coarse) particles. The designations for the examined particle-size distributions include 45-55, 48-52, 50-50, 52-48, and 60-40 (coarse percentage-fine percentage) as presented in Table 4. The particle-size distributions used in this study were selected to identify the proportions at which the specimen behavior is dominated by one proportion or the other according to percolation theory (Peters and Berney 2010). The stress-strain plots for the triaxial tests run in this investigation at 15 psi and 50 psi are presented in Figures 14 and 15, respectively.

O'Sullivan et. al (2006) observed a stiff initial response until the peak strength was achieved, followed by localization formation at the origination of shear planes and dilation in triaxial testing of ideal spheres. Similar results were obtained in this study as shown in Figure 14 through Figure 17. The stainless steel assemblies exhibited stiff initial response followed by localization and dilation. In this study, at a confining stress level of 15 psi the stiffest blends were the 40-60, the weakest were the 60-40, and the blends approaching the percolation threshold purposed by Peters and Berney (2010) fell in the middle. At 50-psi confining pressure the blends 40-60 and 60-40 exhibited the least shear strength and the blends approaching the percolation threshold displayed greatest stiffness. Slight differences in behavior with increasing proportions of large particles were observed.

Table 4. Target number of spheres for consolidated laboratory specimen.

Particle Fraction % (coarse to fine)	Number of 0.75-in.-diam Particles	Number of 0.1875-in.-diam Particles
0-100	0	19,091
40-60	126	12,500
45-55	148	11,475
48-52	153	11,023
50-50	162	10,568
52-48	171	10,114
60-40	198	8,295

At the conclusion of testing on bimodal blends of stainless steel spheres, the testing protocol was extended to bimodal blends of polypropylene and stainless steel sphere mixtures. The large proportion (0.75-in. diam) of these blends was composed of polypropylene spheres and the small proportion (0.1875-in. diam) was stainless steel spheres. The previous series of tests focused on the influence of particle-size distribution, while the polypropylene/stainless steel series attempted to examine the influence of particle stiffness. Many common engineering materials including soils and asphalt concrete are composed of materials with considerably different stiffness properties. An identical testing procedure was conducted for the polypropylene/stainless steel blends as described for the stainless steel bimodal blends. The stress-strain plots for the triaxial tests run in this investigation at 15 psi and 50 psi are presented in Figure 16 and Figure 17, respectively as averages of two replicates conducted for each mixture.

The bimodal blends of polypropylene and stainless steel spheres exhibited similar performance trends as compared to the assemblies of only stainless steel spheres with stiff initial response, followed by localization formation, and dilation. However, due to the reduced stiffness of the large proportion composed of polypropylene spheres, increasing the large proportion resulted in a decrease of both strength and stiffness. Most of the specimens reached 10 percent axial strain without failure. The behavior exhibited by the polypropylene/stainless steel blends followed expectation. The blends with a greater proportion of the large fraction exhibited reduced stiffness and a reduced propensity to dilate with the 60-40 blend exhibiting continued consolidation through 10 percent shear strain, then switching to a dilative state. Also dissimilar from the stainless steel only tests, a distinct difference in behavior can be observed with increasing large (soft) proportion.

Figure 14. Stress-strain behavior of stainless steel spheres at 15 psi.

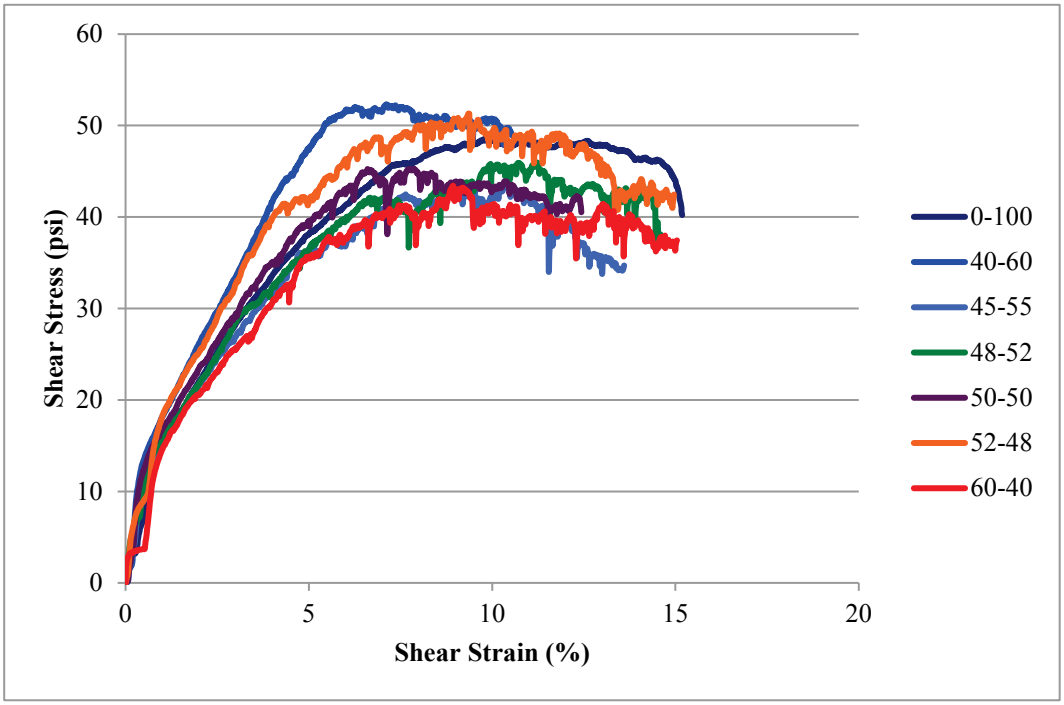

Figure 15. Stress-strain behavior of stainless steel spheres at 50 psi.

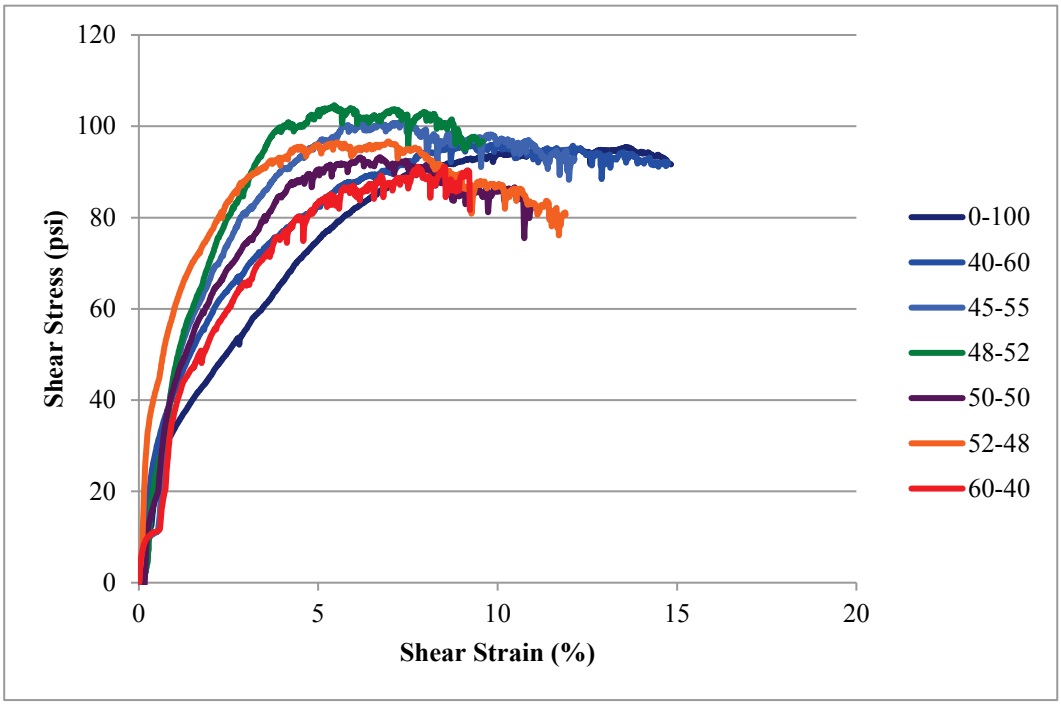

Figure 16. Stress-strain behavior of polypropylene/ stainless steel spheres at 15 psi.

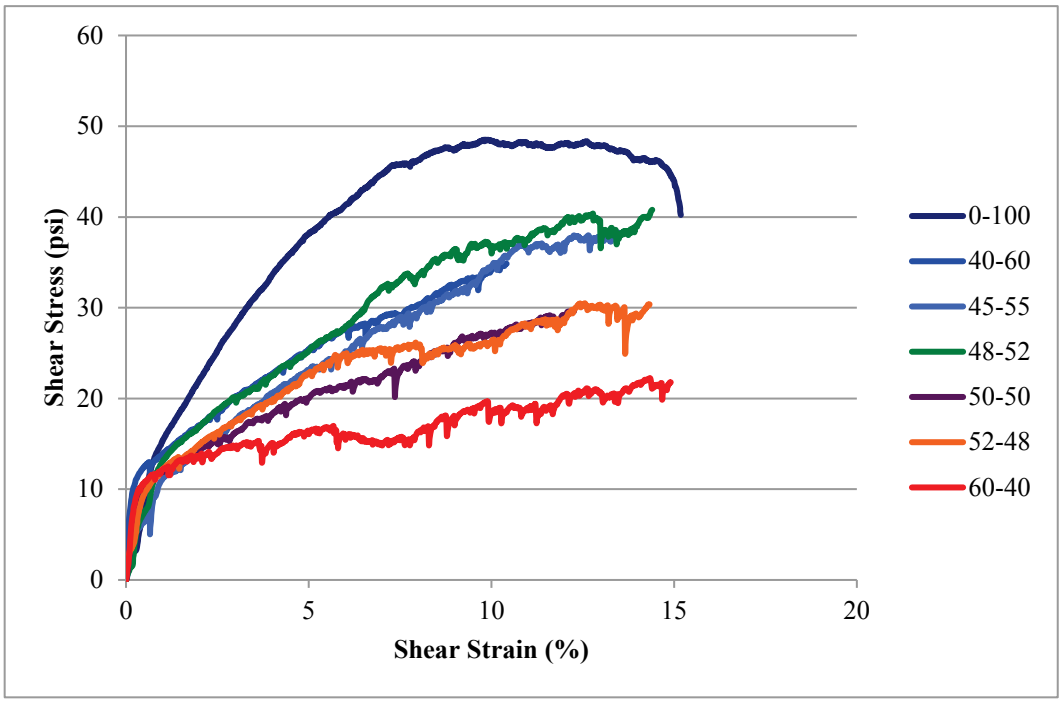

Figure 17. Stress-strain behavior of polypropylene/ stainless steel spheres at 50 psi.

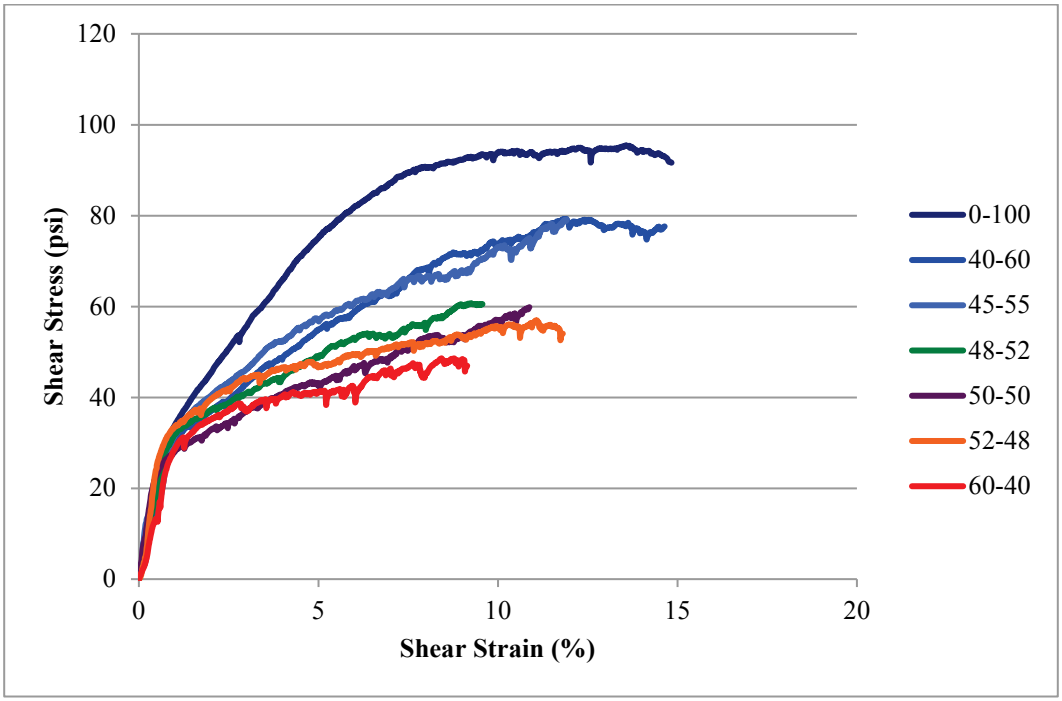

4.3 Naturally occurring particles

The use of uniform spheres allows for the generation of numerical models that accurately represent the simulated particle geometry. Numerical simulations provide valuable data on the micromechanics of particulate systems that is unattainable using standard laboratory measures. However, naturally occurring particles that are commonly used in engineering applications deviate greatly from easily represented ideal shapes (spheres, cubes etc.). The use of ideally shaped particles (spheres) to investigate the micromechanical response of naturally occurring particles was investigated in this study. Although the geometry of the particles is not accurately represented, the application of the DEM model can still provide valuable information on the behavior of particulate assemblies of interest. Laboratory testing of naturally occurring materials was not pursued as part of this investigation. However, laboratory data published by Peters and Berney (2010) on bimodal particle distributions of sand and silty-clay were examined and provided a platform to calibrate the DEM model and validate the laboratory observed engineering behavior. This process provided the necessary guidance to calibrate the polypropylene and steel materials used in this study.

Peters and Berney (2010) investigated the constitutive response of gap-graded binary mixtures at critical mixture ratios. Important engineering materials including flexible pavements, low permeability retaining structures, and filters are often approximated as gap-graded particle-size distributions. The study focused on a laboratory study of gap-graded materials analyzed using modern micro-mechanical research techniques. The central theme of the work was the identification of a critical mixture ratio identified using percolation theory.

4.3.1 Summary of testing presented by Peters and Berney

The mechanical behavior of binary mixtures composed of sand and silty-clay as the relative fraction of each material was examined by Peters and Berney (2010). Triaxial compression testing was conducted on 1.4-in.-diam by 3.0-in.-tall cylindrical specimens of USCS classified SP sand and CL silty-clay. The specimens were compacted using a pneumatic kneading compactor with tip forces ranging from 5 to 60 psi. The specimens were tested in a triaxial apparatus in accordance with ASTM standard test method D 4767 (ASTM 2004). The researchers found evidence of the percolation threshold at sand fractions between 45 and 48 percent. Mixtures having reached the threshold displayed erratic, even unstable behavior with respect to expected mechanical response. The traditional relationship between mean stress and void ratio based on the critical state theory was also observed to break down as the coarse material nears its threshold fraction (Peters and Berney 2010). Additionally, the sand fraction controlled the achievable compaction in the silty-clay fraction. The authors concluded that the observed behavior was due to the development and evolution of force chains and not a reduction in void ratio caused by increased confining pressure.

4.3.2 Testing results

Results of laboratory testing as presented by Peters and Berney (2010) were used to calibrate and validate DEM simulations of assemblies of particles representing a bimodal sand/silty-clay blend. The stress-strain response of binary blends of sand and silty-clay at 15 psi and 50 psi was reproduced using data from Peters and Berney (2010) and is presented in Figures 18 and 19. Characteristic curves developed using uniform assemblies of sand and silty-clay were used to calibrate the DEM model prior to the simulation of sand/silty-clay bimodal blends and are presented in Figure 18 through Figure 20.

Figure 18. Stress-strain behavior of sand and silty-clay blends at 15 psi used in Peters and Berney (2010) study.

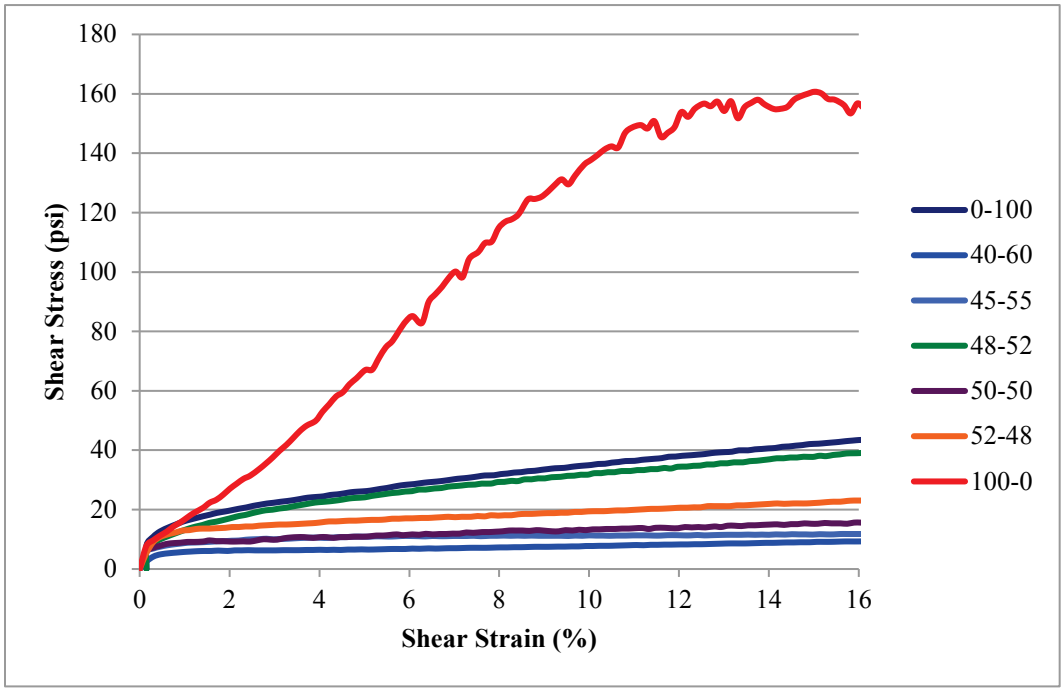

Figure 19. Stress-strain behavior of sand and silty-clay blends at 50 psi used in Peters and Berney (2010) study.

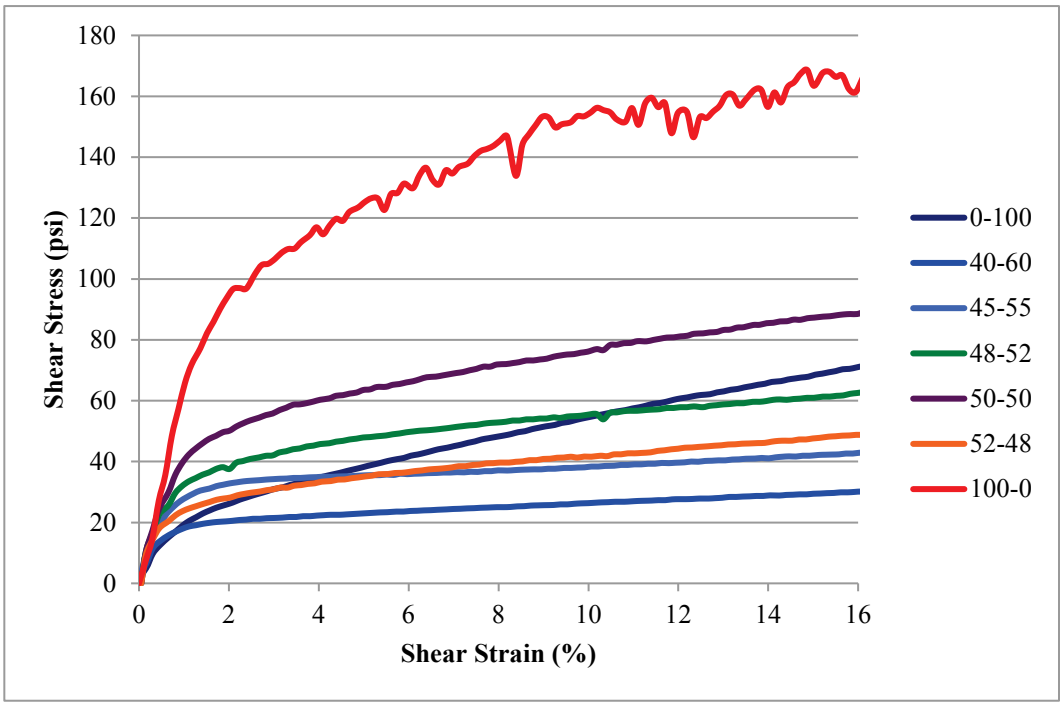

Figure 20. Stress-strain behavior of sand and silty-clay calibration curves.

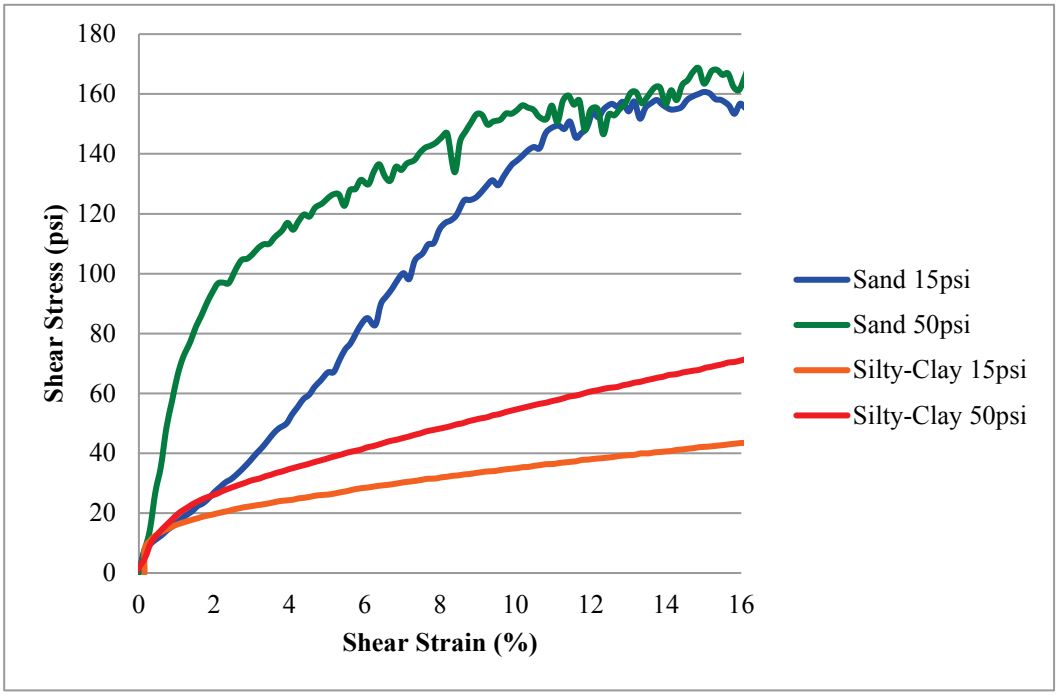

5 Numerical Simulation of Bimodal Systems

5.1 Testing program

The objective of the numerical simulations was to develop assemblies of consolidated spheres that exhibit similar mechanical behavior as the specimens examined in laboratory testing and to use the specimens to investigate the stress transfer mechanisms occurring in bimodal particulate systems undergoing shear. The intention was not to develop the most physically realistic numerical model but to build one from which meaningful data on the particulate mass could be obtained. Simulations were made of varying particle-size distributions composed of stainless steel and polypropylene/stainless steel spheres as outlined in Chapter 4. Simulation of natural soil materials composed of bimodal blends of sand and silty-clay was also attempted using data obtained from Peters and Berney (2010).

The DEM model developed by Horner et. al (2001) was used to generate particulate specimens and simulate the consolidated-undrained triaxial compression testing of cubical assemblies of particles. The DEM model consisted of a finite modeling space, confining walls, and approximately 7,000 spherical particles. Using any more particles in the DEM model proved too time consuming and difficult for the computer systems to process and so a compromise was made at 7,000 to enable this initial study to continue. The finite modeling space allowed for tracking of the model elements between computational time increments. The confining walls were composed of 3-D facets defined similarly to finite elements and representing rigid objects. The spherical particles were elastic, indestructible elements defined by the location of the centroid, particle radius, and specific gravity. The spherical particles are the primary elements of interest that provide data on inter and intra-particle forces occurring in the consolidated granular assembly.

5.1.1 Specimen generation

Consolidated assemblies of spheres were subjected to simulated triaxial compression testing to determine the micro-level performance of varying size distributions of particulate materials. The specimens were generated using a growth algorithm followed by isotropic consolidation. Once initiated, the DEM model generated an assemblage of uniform particles within

the model space with diameters equal to the largest target particle size. A growth algorithm then randomly selects particles in the assembly, based upon the number of particles required to reach the desired size distribution, and decreases the size of the selected particles with each computational time-step until the target size is reached. Cui and O'Sullivan (2006) observed that randomly generating specimens in the numerical environment results in slight perturbations in material fabric. This effect can be exaggerated by the use of low particle counts. However, the researchers found that macro performance was not significantly influence by the minor differences in fabric.

Concurrent with the change in particle size, the six confining walls begin moving towards the center of the model space under fixed velocity control. As the rigid walls impact the particles contained within, the particles are forced together forming the consolidated specimen. Maximum density is reached when no changes in specimen dimensions occur with additional computational time-steps.

The particle sizes used in the DEM model were 0.80 and 0.20 in. diam with size distributions similar to those described in Chapter 4 and shown in Table 5. The number and size of particles used in the numerical model compare favorably to the ideal spheres used in physical testing (0.75 and 0.1875 in.). However, the sand and silty-clay grains used by Peters and Berney (2010) had average diameters of 0.086 and 0.0001 in., respectively. Their 3.0- by 1.4-in. cylindrical triaxial specimens contained an average 4,500 sand or 7.3×10^{10} silty-clay particles. The simulation of a representative specimen of the silty-clay particles was not possible due to the prohibitive computational expense (Bathurst and Rothenburg 1988). Additionally, one to one correspondence between computational and physical particle size is not necessary, because the employed test bed represents a representative elemental volume of particles that approximates the mechanical response of the prototype medium rather than being a faithful rendition of micromechanical behavior (Horner et. al 2001).

Table 5. Sphere distribution for numerical model consolidated specimen.

Particle Fraction % (coarse to fine)	Number of 0.80-in.-diam Particles	Number of 0.20-in.-diam Particles
0-100	0	6,859
40-60	37	6,060
48-52	72	6,621

Particle Fraction % (coarse to fine)	Number of 0.80-in.-diam Particles	Number of 0.20-in.-diam Particles
50-50	93	6,673
52-48	106	6,675
60-40	165	6,672

5.1.2 Consolidation of particles

Once a specimen of consolidated spheres at the maximum possible density was generated, the next step was to achieve the desired volumetric and confining stress states prior to simulating triaxial compression testing. During the initial growth and consolidation, the spheres within the specimen were assigned the material properties of stainless steel. However, for the polypropylene/stainless steel and sand/silty-clay blends, the material properties of the spheres were modified prior to transforming the specimen further using the values presented in Table 6. After the desired particle properties were assigned, the confining walls were relaxed until the desired confining stress was obtained. The walls were relaxed by switching from velocity to force control and specifying the force required to reach a confining stress of either 15 or 50 psi. Evans et al. (2009) observed that it is difficult to generate specimens with exact values of both confining stress and void ratio. The same phenomenon was experienced in this study. The objective of this investigation was to examine the stress transfer mechanisms occurring in consolidated particulate specimens that are strongly influenced by the initial stress state. Therefore, the relaxation process was discontinued when the average stress on the consolidated assembly reached the target level ±10 percent.

Table 6. Particle properties for materials simulated in DEM model.

	Stainless Steel	Polypropylene	Sand	Silty-Clay
Specific gravity	7.80	0.90	2.65	2.70
Normal stiffness (ksi)	29,000	290	6,600	30
Shear stiffness (ksi)	29,000	290	6,600	30
Rolling resistance	0.0	0.0	7.0	0.0
Torsion resistance	0.0	0.0	7.0	0.0
Translational friction	0.60	0.80	0.70	1.20
Rotational friction	0.60	0.80	0.70	1.20

Cui and O'Sullivan (2006) found in constructing numerical model specimens that obtaining an exact replica of physical specimens was not possible. Typically, the void ratio of numerical specimens was slightly lower

than specimens constructed in the laboratory. The observation of Cui and O'Sullivan (2006) was replicated for the coarse polypropylene/stainless steel and all of the sand/silty-clay blends, but the opposite was observed for the stainless steel and fine polypropylene/stainless steel blends examined in this study. Evans et al. (2009) comment that the relative density across specimens should be approximately the same even if the void ratios vary slightly when the specimen are generated and consolidated using an identical method. An example of a consolidated cubical specimen is presented in Figure 21. The volumetric properties of the stainless steel, polypropylene/stainless steel, and sand/silty-clay numerical model specimens are presented in Tables 7 through Table 9 respectively. Because each mixture consisted of the same number of particles, uniform mixtures of all one size fraction (0-100) exhibited a taller structure, because the developing DEM with all one particle size occupies a greater solid volume than binary mixtures, where many smaller particles were present to reduce the overall solid volume.

Figure 21. Consolidated specimen of uniform spheres.

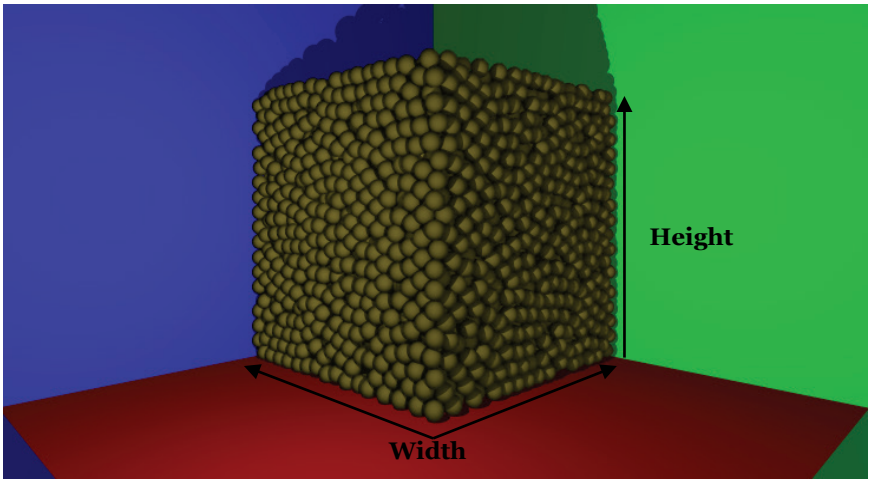

Table 7. Volumetric properties of numerical model stainless steel blends.

Particle Fraction % (coarse to fine)	15 psi			50 psi		
	Width (in.)	Height (in.)	Void Ratio	Width (in.)	Height (in.)	Void Ratio
0-100	14.4	14.5	0.65	14.3	14.4	0.61
40-60	3.6	3.7	0.74	3.3	3.3	0.52
48-52	3.9	3.9	0.68	3.7	3.7	0.54
50-50	3.9	3.9	0.55	3.8	3.8	0.45
52-48	4.2	4.2	0.61	3.9	3.9	0.42
60-40	4.3	4.3	0.44	4.3	4.3	0.43

5.1.3 Simulation of triaxial testing

The consolidated-undrained triaxial compression testing was simulated using the DEM model. A zero volume change confining cell was used to approximate the effect of the undrained triaxial compression testing. The confining cell was composed of six rigid bounding walls composed of facet elements. The confining walls are frictionless to ensure that normal boundary induced stresses (Belheine et al. 2009) occur within the particulate assembly.

Table 8. Volumetric properties of numerical model polypropylene/ stainless steel blends.

Particle Fraction % (coarse to fine)	15 psi			50 psi		
	Width (in.)	Height (in.)	Void Ratio	Width (in.)	Height (in.)	Void Ratio
0-100	14.4	14.5	0.65	14.3	14.4	0.61
40-60	3.6	3.7	0.74	3.3	3.4	0.54
48-52	3.8	3.8	0.60	3.6	3.7	0.50
50-50	3.9	3.9	0.51	3.8	3.8	0.44
52-48	3.9	3.8	0.40	3.8	3.8	0.40
60-40	4.2	4.2	0.41	4.3	4.3	0.41

Table 9. Volumetric properties of numerical model sand/silty-clay blends.

Particle Fraction % (coarse to fine)	15 psi			50 psi		
	Width (in.)	Height (in.)	Void Ratio	Width (in.)	Height (in.)	Void Ratio
0-100	14.0	14.2	0.58	13.5	13.7	0.44
40-60	3.3	3.4	0.58	3.2	3.3	0.41
48-52	3.7	3.7	0.54	3.5	3.5	0.41
50-50	3.8	3.8	0.49	3.6	3.6	0.38
52-48	3.9	3.9	0.44	3.7	3.8	0.36
60-40	4.2	4.2	0.40	4.2	4.2	0.40

The bottom wall was held stationary, simulating the pedestal of the physical triaxial cell. The top wall moved toward the bottom wall at a fixed rate under velocity control, simulating the downward movement of the physical top platen under the force of the axial loading piston. To maintain the zero volume change environment of undrained triaxial compression testing, for each increment of vertical displacement, the lateral confining walls moved outward from the centroid of the specimen one-half (1/2) the vertical displacement of the top wall. The confining walls relaxed outward

allowing the particulate assembly to deform both vertically and radially, simulating the confinement provided by the neoprene membrane and applied effective confining pressure in physical triaxial compression testing.

The simulated testing was continued for a fixed number of computational increments (200,000) resulting in 7.0 to 9.0 percent shear strain in the numerically modeled specimens. Modeling of water is not currently possible using the DEM model. Therefore, the pore-water pressure (μ) of the numerical model specimens was approximated by subtracting the theoretical total mean stress from the effective mean stress as shown in Equation 20.

$$\mu = \frac{\sigma_1 + 2\sigma_3}{3} - \left(\frac{\sigma_1 - \sigma_3}{3} - \sigma_3 \right) \tag{20}$$

where:

σ_1 = principal stress measured on the top wall

σ_3 = confining pressure calculated as the average stress on the four lateral confining walls.

Data obtained from the DEM model included the relative position, displacement, force, moment, and orientation of each element (spherical particles and confining walls) within the modeling space at every computational increment.

5.2 Testing results

Data were extracted from the DEM model at selected intervals to include 1, 10, 100, 1,000, 10,000, 50,000, 100,000, 150,000, and 200,000 computational increments. The data extracted from the model included the location and force acting on each of the six confining walls and each of the approximately 7,000 particles. The location and force acting on the confining walls were used to calculate the shear stress, total mean stress, effective mean stress, shear strain, and pore-water pressure. The confining walls were used to approximate the macroscale properties of the consolidated specimen that would traditionally be determined in physical triaxial compression testing. The location and forces acting on the individual par-

ticles provided data not available in standard laboratory testing to include the distribution of stresses within discrete particle-size fractions and the evolution of coordination number during shearing.

5.2.1 Macroscale mechanical properties

The macroscale mechanical properties of each specimen determined during simulated triaxial compression testing included shear stress, total mean stress, effective mean stress, and shear strain, calculated using Equations 21 through 24, respectively. The equation for determining the pore-water pressure (Equation 20) was presented previously.

$$\sigma_{shear} = \sigma_1 - \sigma_3 \tag{21}$$

where:

σ_{shear} = shear stress

σ_1 = principal stress measured on the top wall

σ_3 = confining pressure calculated as the average stress on the four lateral confining walls.

$$\sigma_{total\ mean} = \frac{\sigma_{shear}}{3} + \sigma_3 \tag{22}$$

where $\sigma_{total\ mean}$ is the total mean stress.

$$\sigma'_{mean} = \frac{\sigma_1 + 2\sigma_3}{3} \tag{23}$$

where $\sigma_{effective\ mean}$ is the effective mean stress.

$$\varepsilon_{shear} = 1.5 * \varepsilon_{axial} \tag{24}$$

where ε_{shear} is the shear strain and ε_{axial} is the axial strain measured as the change in distance divided by the initial distance between the top and bottom confining walls.

5.2.1.1 Model calibration

The first series of numerical simulations was run to calibrate the DEM model. The characteristic curves developed using uniform assemblies of 0.1875-in. spheres or uniform assemblies of sand/silty-clay, as presented in Chapter 4, were used to calibrate the DEM model. For each material investigated in this study (stainless steel, polypropylene, sand, and silty-clay) the material properties of the model were established as presented in Table 6. The simulated triaxial compression testing was run for 200,000 computational increments at both 15- and 50-psi effective confining stress with data extracted at the previously presented intervals. The extracted data were used to generate stress-strain, shear/principal stress (q-p), and pore-water pressure plots. The data from the simulated testing were compared to the characteristic curves developed from physical laboratory testing and an iterative refinement process ensued until similar mechanical behavior was observed. The final calibrated material properties are presented in Table 10. Comparisons of the stress-strain behavior of the physical and numerical tests are presented in Figure 22 and Figure 23 for the ideal spheres and naturally occurring materials, respectively, where the physical test data are represented with a solid line and the numerical test data are represented with a dashed line.

Table 10. Calibrated particle properties for materials simulated in DEM model.

	Stainless Steel	Polypropylene	Sand	Silty-Clay
Specific gravity	7.80	0.90	2.65	2.70
Normal stiffness (ksi)	10,000	1,500	10,000	1,200
Shear stiffness (ksi)	10,000	1,500	10,000	1,200
Rolling resistance	0.0	0.0	7.0	0.0
Torsion resistance	0.0	0.0	7.0	0.0
Translational friction	0.30	0.35	0.30	0.50
Rotational friction	0.30	0.35	0.30	0.50

5.2.1.2 Model validation

Once the numerical model was calibrated using the physical triaxial compression testing data, validation of the model was pursued by examining bimodal particle-size distributions similar to those examined in the laboratory. The specimens were generated and tested as described previously in the “Testing program” section. Initially, blends of 40 percent (by volume) 0.8-in.-diam spheres and 60 percent 0.2-in.-diam spheres were examined at both 15-psi and 50-psi effective confining pressure. Macro-scale behav-

ioral plots were developed including stress-strain, shear/mean stress (q-p plot), and pore-water pressure using Equations 20 through 24. This process was repeated for increasing proportions of 0.8-in. diam particles. The designations for the examined particle-size distributions included 40-60, 48-52, 50-50, 52-48, and 60-40. The stress-strain plots for the numerically simulated triaxial compression tests run in this investigation at 15 and 50 psi are presented in Figure 24 and Figure 25 for the stainless steel blends, Figure 26 and Figure 27 for the stainless steel/polypropylene blends, and Figure 28 and Figure 29 for the sand/silty-clay blends.

Figure 22. Stress-strain behavior of physical (solid) and model (dashed) uniform spheres.

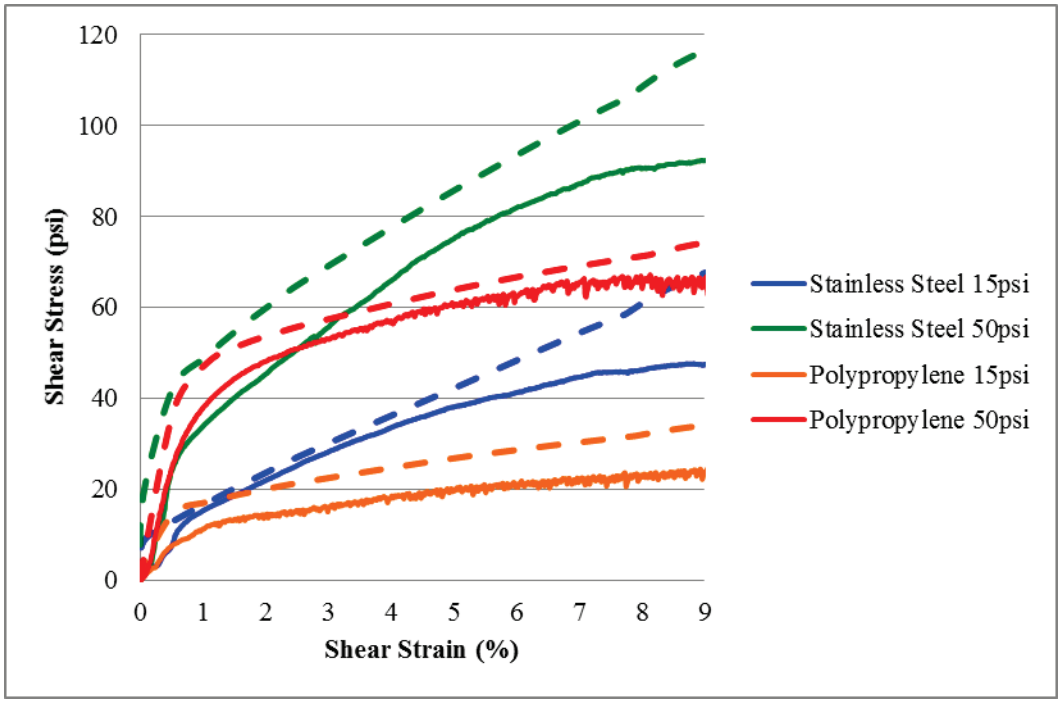

Figure 23. Stress-strain behavior physical (solid) and model (dashed) sand/silty-clay materials from Peters and Berney (2010) study.

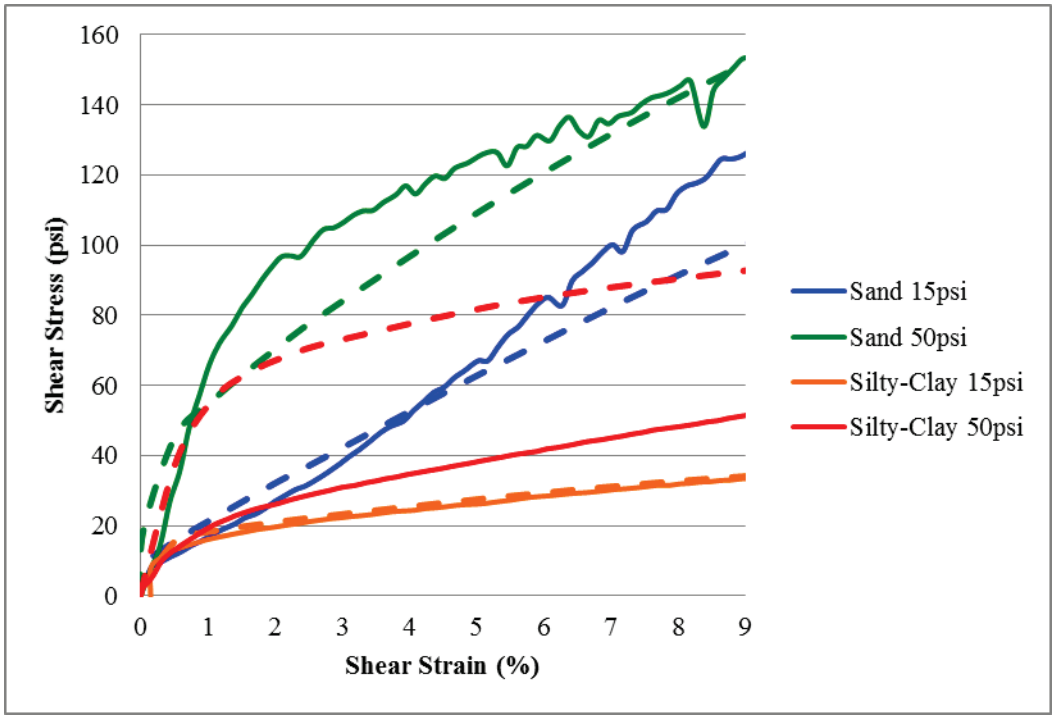

Figure 24. Stress-strain behavior of simulated stainless steel spheres at 15 psi.

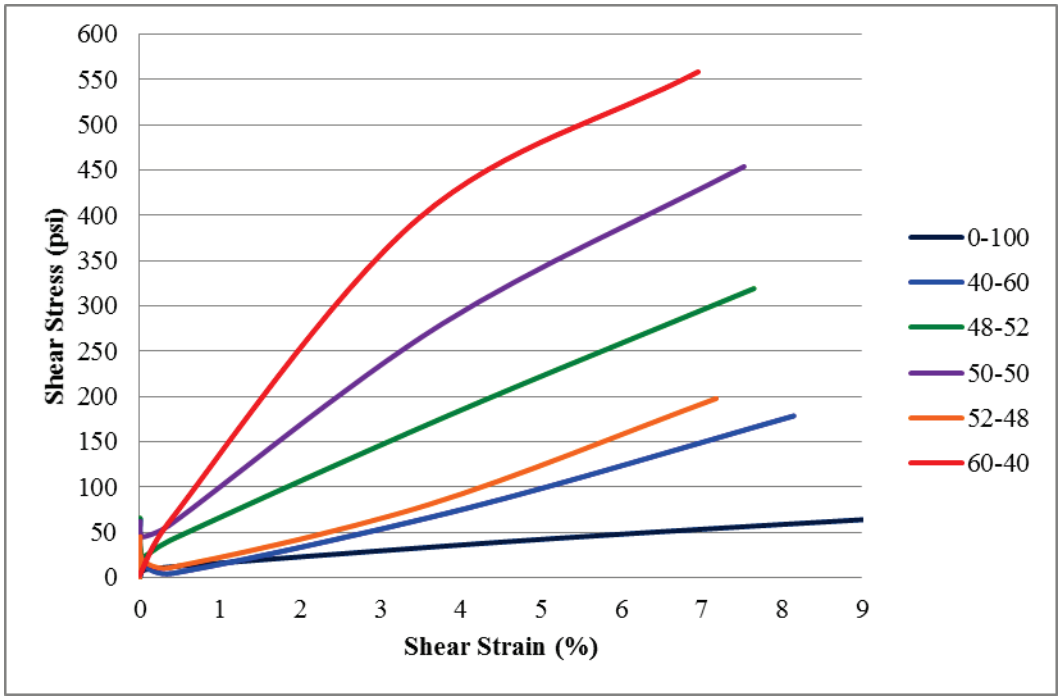

Figure 25. Stress-strain behavior of simulated stainless steel spheres at 50 psi.

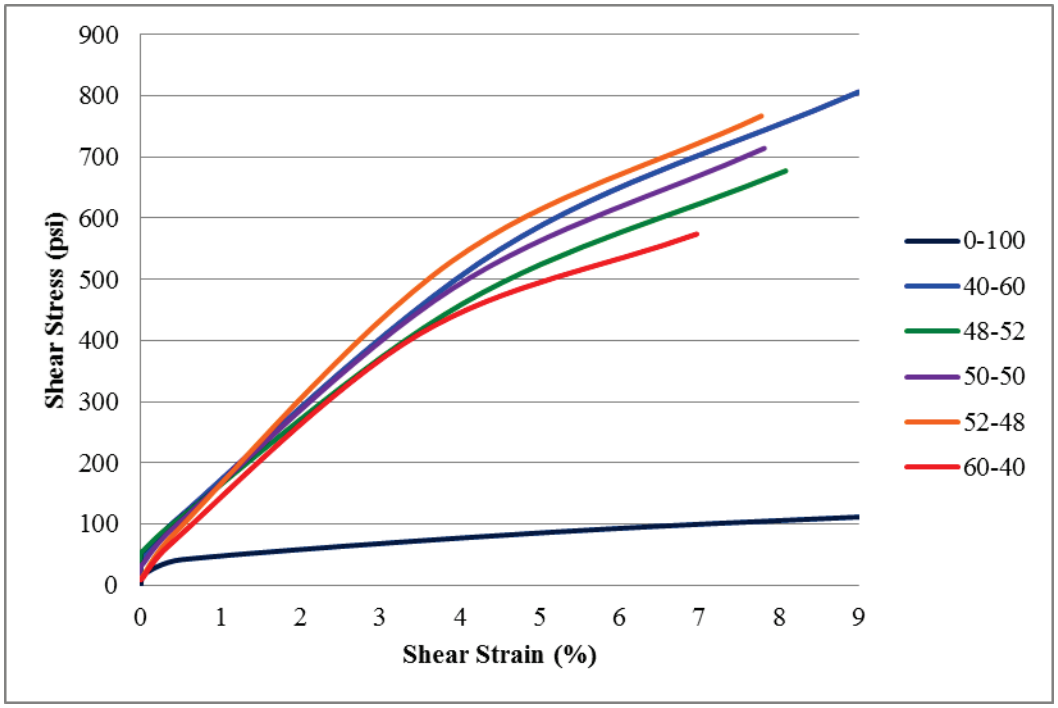

Figure 26. Stress-strain behavior of simulated polypropylene/ stainless steel spheres at 15 psi.

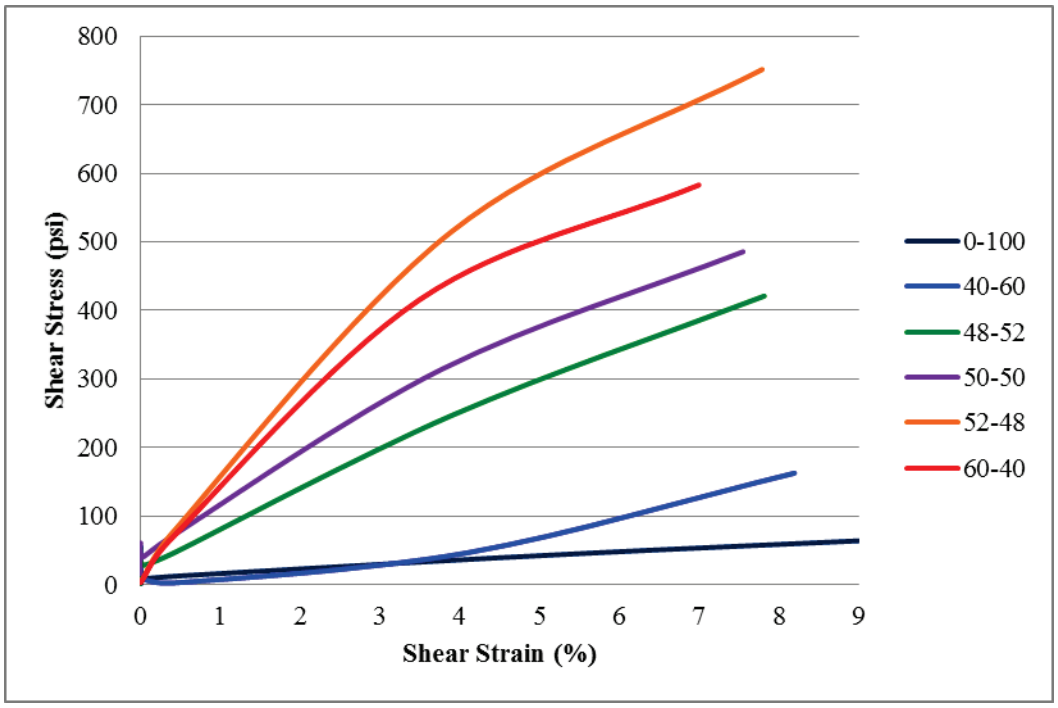

Figure 27. Stress-strain behavior of simulated polypropylene/ stainless steel spheres at 50 psi

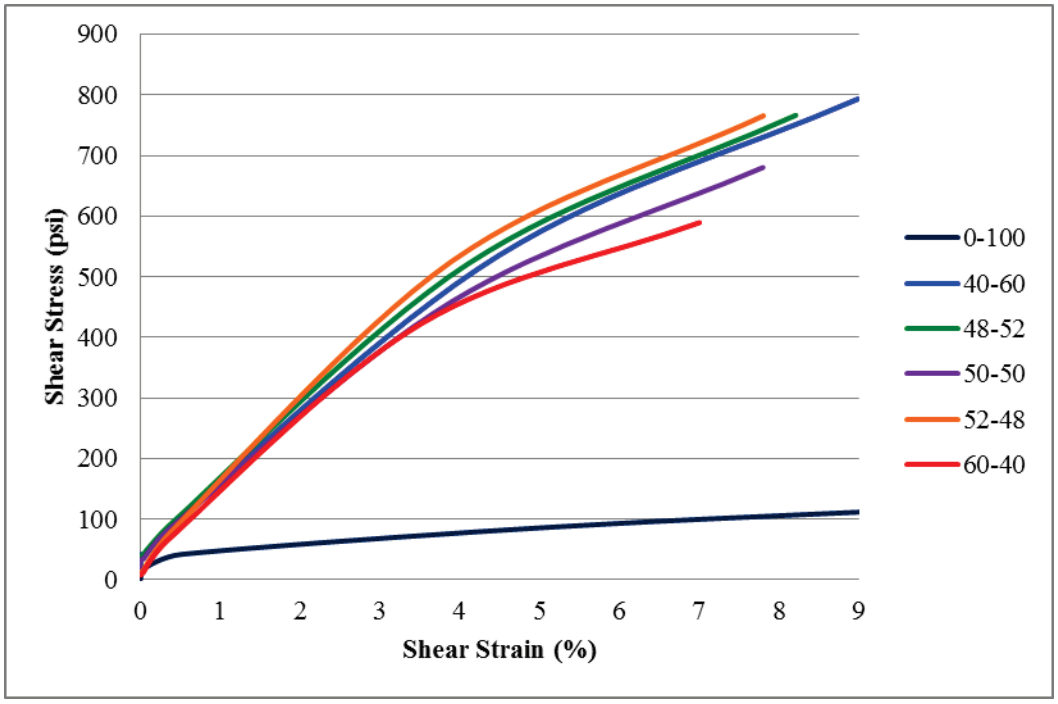

Figure 28. Stress-strain behavior of simulated sand/ silty-clay spheres at 15 psi

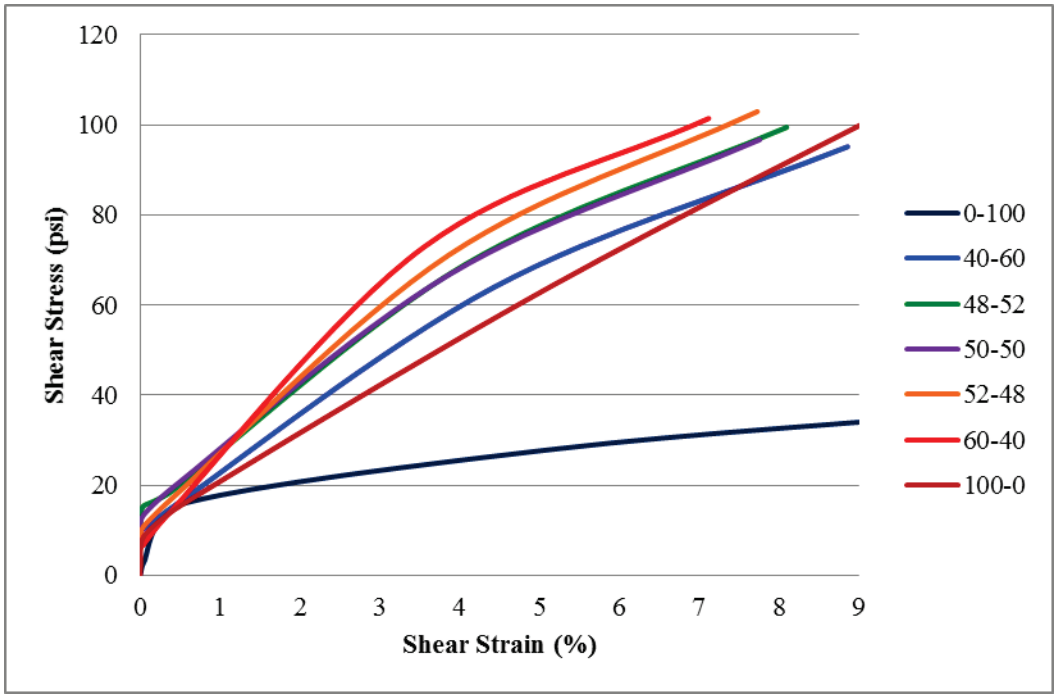

Figure 29. Stress-strain behavior of simulated sand/ silty-clay spheres at 50 psi.

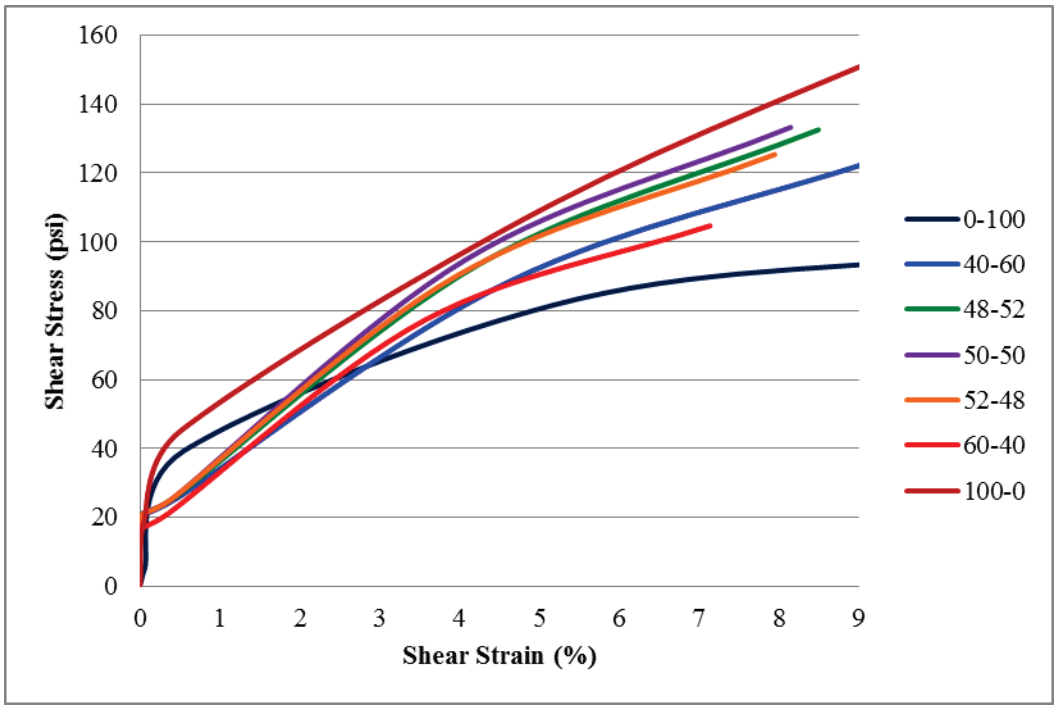

In examining these stress-strain plots, the influence of confining stress is immediately apparent. At low confining pressures (15 psi), the differences in mechanical behavior between different bimodal gradations is pronounced. At high confining pressures (50 psi), the behaviors become more simular. Trends in observed mechanical performance appear to be more greatly influenced by confining pressure than material type. Regardless of composing material, at 15-psi confining pressure the 40-60 blend displayed the weakest shear strength and at 50 psi, the 60-40 blend appeared the weakest. Clearly defined relationships between increased large particle proportion and shear strength at both high and low confining pressure levels were not observed for any of the bimodal materials investigated. When compared to the laboratory triaxial testing data on spherical particles, the simulations run at the low confining stress (15 psi) displayed inverse behavior. However, the simulations run at the high confining pressure (50 psi) displayed similar strength trends as compared to the laboratory results. Differences in expected behavior are likely due to the limited number of particles in the DEM, which allow boundary conditions to influence the dilative characteristics within the simulation at the lower confining pressures.

5.2.2 Microscale mechanical properties

The primary advantage of employing numerical testing methods is the availability of particle scale data not easily obtained in physical testing. The stresses acting on and connectivity of each particle within the compacted assembly are data available only through employment of numerical testing methods. The average normal and shear stress acting on each particle are determined by summing the forces acting at each contact that a given particle participates in as shown in Equation 25.

$$\sigma_{ij}^{P} = \frac{1}{V^{P}} \sum_{c=1}^{N_c} r_j^c f_i^c \tag{25}$$

where:

σ_{ij}^{p} = average stress tensor component

V^{P} = volume of the particle

N_c = number of contacts the particle participates in

r_j^c = distance from the particle centroid to the point of contact

f_i^c = force at the contact

A simplified 2-D schematic of the relationship presented in Equation 25 is presented in Figure 30.

Figure 30. Schematic of contact force components.

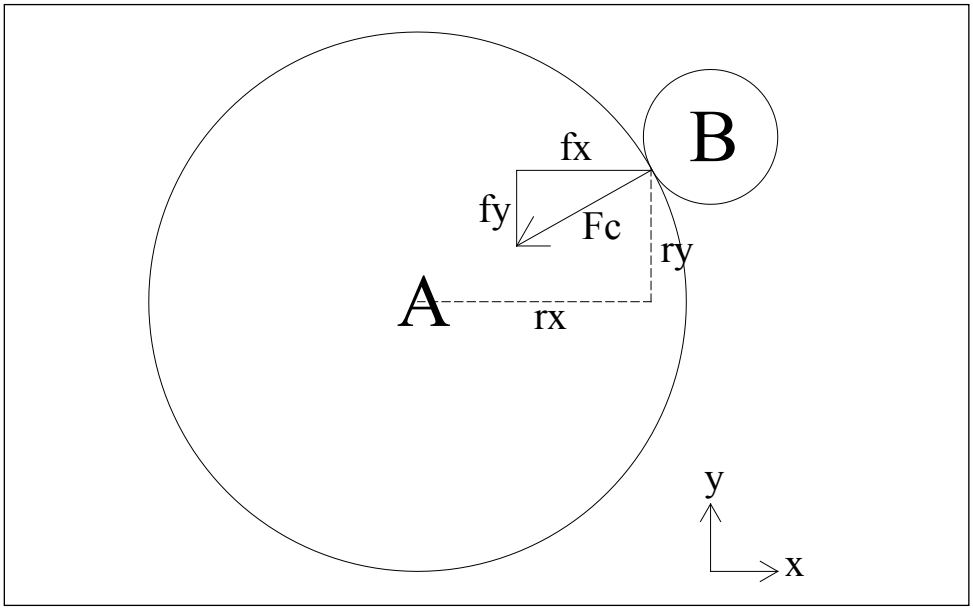

Equation 25 is used to describe the component normal and shear stresses that define the stress tensor for each particle. The component stresses were used in this study to calculate the effective mean and shear stresses for each particle in the assembly as shown in Equations 26 and 27.

$$\sigma_{effective\ mean} = \frac{\sigma_{xx} + \sigma_{yy} + \sigma_{zz}}{3} \tag{26}$$

where

$\sigma_{effective\ mean}$ = effective mean stress

σ_{xx} = normal stress in the *x*-direction

σ_{yy} = normal stress in the *y*-direction

σ_{zz} = normal stress in the z-direction

$$\sigma_{shear} = \frac{\sqrt{\sigma_{xy}^{\ 2} + \sigma_{xz}^{\ 2} + \sigma_{yz}^{\ 2}}}{3} \tag{27}$$

where:

σ_{shear} = shear stress

σ_{xy} = x-y shear stress component

σ_{xz} = x-z shear stress component

σ_{yz} = y-z shear stress component

5.2.2.1 Distribution of stresses

The distribution of stress amongst the particle-size fractions of a bimodal blend provides insight into the proportion that is dominating engineering behavior. The normal and shear stresses were averaged for each particle size for the bimodal blends investigated in this study. The comparisons of average stress within each particle-size fraction for the stainless steel, polypropylene/stainless steel, and sand/silty-clay numerical specimen after consolidation at both 15- and 50-psi effective confining pressure are presented in Figure 31 through Figure 33, respectively.

Figure 31. Shear stress distribution for polypropylene/stainless steel specimens at 15 psi (left) and 50 psi (right) confining pressure.

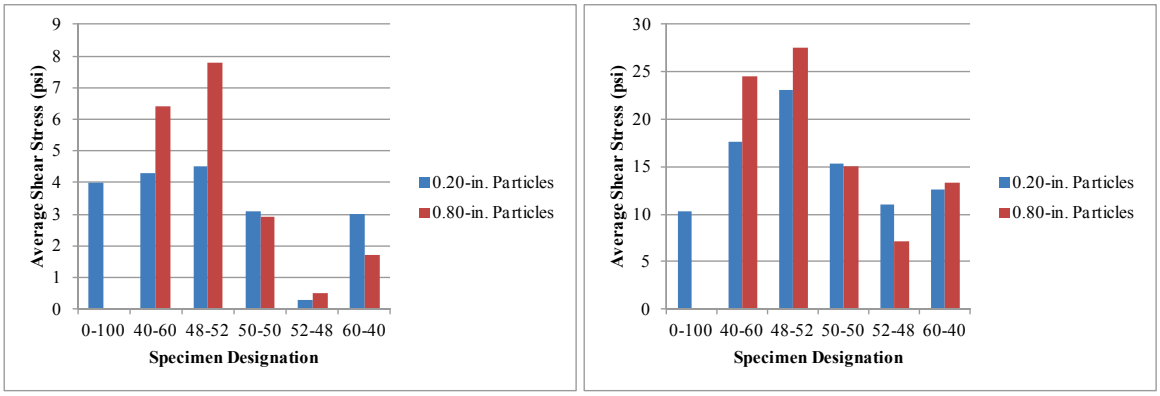

Figure 32. Shear stress distribution for stainless steel specimens at 15 psi (left) and 50 psi (right) confining pressure.

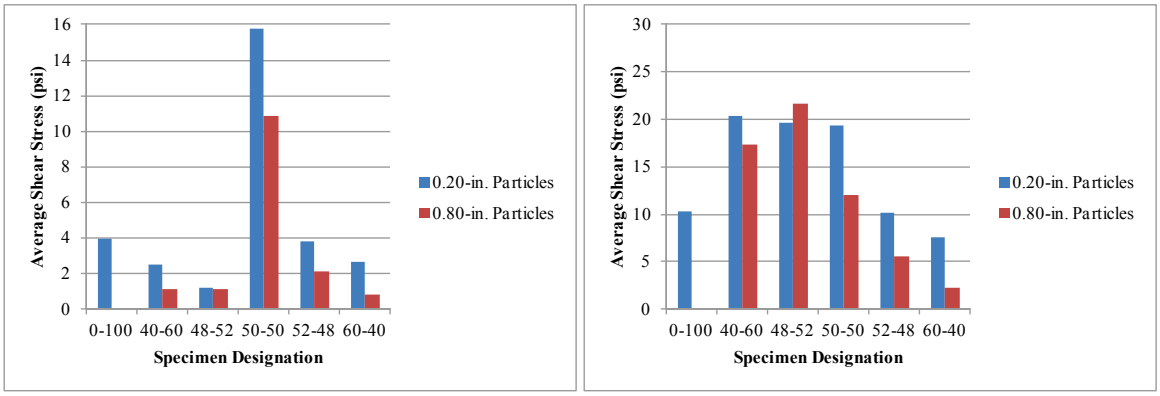

Figure 33. Shear stress distribution for sand/silty clay specimens at 15 psi (left) and 50 psi (right) confining pressure.

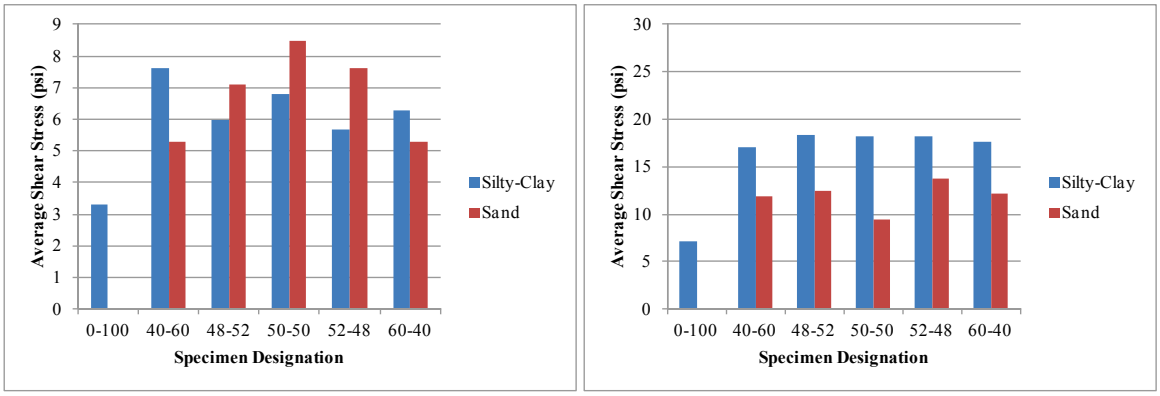

Clear trends when examining the distribution of stress amongst the discrete particle-size fractions are not observed following isotropic consolidation (Figures 32 and 33). A state of stress equilibrium is approached at both 15 and 50 psi for the stainless steel assemblies blended at or near 50-50 and the polypropylene/stainless steel assemblies blended at 48-52. No stress equilibrium state is observed for the bimodal sand/silty clay blends investigated in this study. During shear, regardless of particle-size distribution or composing material type, the majority of the stress is transmitted through the small size fraction.

5.2.2.2 Coordination number

Coordination number is simply a measure of the number of contacts a given particle participates in. The average coordination number for a specimen is the total number of contacts in the assembly divided by the number of particles. The average coordination number provides an indication of the connectivity of the assembly and also provides an indication of the development of force chains. An increase in average coordination number is commonly observed during consolidation. As the particles are forced closer together the number of contacts increases. During dilation, the specimen is increasing in volume, reducing the density of particles and subsequently, the coordination number. As force chains develop, the coordination number of the participating particles increases, while the coordination number of particles not participating in the force chain decreases. The average total coordination number, average large proportion coordination number, and average small proportion coordination number following isotropic consolidation for the specimens examined in this study at both 15- and 50-psi effective confining pressure are presented in Tables 11 through 13.

Table 11. Coordination number for stainless steel specimens.

Particle Fraction % (coarse to fine)	15 psi			50 psi		
	Total	0.80-in. Particles	0.20-in. Particles	Total	0.80-in. Particles	0.20-in. Particles
0-100	6.2	--	6.2	6.6	--	6.6
40-60	6.6	30.1	6.4	8.5	37.2	8.2
48-52	7.3	36.8	6.9	8.5	43.1	8.0
50-50	7.6	39.4	7.1	8.6	44.3	8.0
52-48	6.7	33.6	6.2	8.8	45.4	8.2
60-40	8.0	39.9	7.2	8.1	40.3	7.3

Table 12. Coordination number for polypropylene/ stainless steel specimens.

Particle Fraction % (coarse to fine)	15 psi			50 psi		
	Total	0.80-in. Particles	0.20-in. Particles	Total	0.80-in. Particles	0.20-in. Particles
0-100	6.2	--	6.2	6.6	--	6.6
40-60	6.8	30.3	6.5	8.5	37.5	8.2
48-52	7.7	38.6	7.3	8.8	44.1	8.3
50-50	7.8	40.3	7.3	8.5	43.9	8.0
52-48	8.8	45.4	8.2	8.9	45.6	8.3
60-40	8.2	41.1	7.4	8.2	41.2	7.4

Table 13. Coordination number for sand/silty clay specimens.

Particle Fraction % (coarse to fine)	15 psi			50 psi		
	Total	0.80-in. Particles	0.20-in. Particles	Total	0.80-in. Particles	0.20-in. Particles
0-100	7.1	--	7.1	8.2	--	8.2
40-60	8.1	36.5	7.8	9.2	40.0	8.9
48-52	8.5	43.8	8.1	9.6	48.2	9.1
50-50	8.4	43.4	7.9	9.5	46.5	8.9
52-48	8.7	45.1	8.1	9.4	48.0	8.7
60-40	8.6	42.9	7.8	8.7	43.1	7.8

As a general trend, total, large proportion, and small proportion coordination number increases with increasing large proportion content. Regardless of material and confining pressure level, the 52-48 blends appear to have the largest total, large proportion, and small proportion coordination numbers. During shear the coordination number for all of the investigated

assemblies decreases, with the greatest decrease occurring in the 60-40 blends.

6 Analysis and Discussion

6.1 Macroscopic behavior

Similar to the observations of O'Sullivan et. al (2006), the DEM model was slightly stiffer and reached peak strength at a lower level of shear strain as compared to laboratory data. However, the DEM model successfully captured volumetric strain response. O'Sullivan et. al (2004) observed that as distribution of particle sizes increases, peak strength decreases and peak strain at failure increases. A definite variation in the response curve was observed to be associated with the standard deviation of the particle-size distribution (O'Sullivan et. al 2006). For the bimodal distributions investigated in this study (Figure 22 through Figure 29), greater shear strength and decreased shear strain were observed for the blends as compared to the uniform assemblies, with the exception of the sand/silty clay blends at 50-psi confining pressure that fell within the large and small particle uniform assemblies (Figure 29). A definite variation in response was observed for the specimens tested at the low confining pressure (15 psi), but the response was more greatly influenced by the coordination number than the distribution of particle sizes.

Cui et. al (2007) observed that polydisperse specimens exhibited greater radial dilation as compared to monodisperse specimens. The same observation was made in this study. The uniform materials investigated in this study including the stainless steel, polypropylene, sand, and silty-clay showed reduced dilative tendency as compared to the bimodal blends. The less stiff materials, polypropylene and silty-clay, exhibited purely contractive behavior, while the stiffer materials, stainless steel and sand, exhibited a short period of contraction followed by dilation. All of the investigated bimodal blends exhibited purely dilative behavior.

Cavarretta et. al (2009) observed that overall response is dominated by the particles participating in force chains. An in-depth investigation into the formation and evolution of force chains was not conducted as part of this study. However, the theory of percolation provides that once the percolation threshold is reached, sufficient coarse particles exist for the formation of force chains. Nearing the percolation threshold is indicated by erratic behavior and a reduction in coordination number. In this

investigation, a clear transition in dominant particle behavior was not observed. Increases in coarse material content resulted in gradual changes in mechanical behavior. However, when examining the sand/silty-clay blends tested at the low confining pressure (15 psi), it can be observed that as coarse particle content increases the stress-strain curve shifts between the uniform fine and uniform coarse assemblies (Figure 28).

The macro-scale response is a function of particle shape, particle size, and void distributions in addition to other internal variables (Thornton 2000). Macro-scale response includes deformability, strength, dilatancy, and strain localization (Belheine et al. 2009). The influences of particle-size distribution and particle stiffness were examined in this study. Distinct changes in response resulting from changes in particle-size distribution were not observed. However, coordination number was found to highly influence material behavior. Additionally, the properties of the material were found to have a less significant influence. The blends composed of stainless steel only and the blends composed of less stiff polypropylene and stainless steel were observed to have similar mechanical response. Common coordination numbers were measured for these blends.

6.2 Microscopic behavior

Stresses calculated from the boundary forces were smaller than the stresses measured internally due to non-uniformities within the specimen (Cui et. al 2007). The bimodal blends examined in this study exhibited contrary behavior. The stresses calculated from the bounding walls were found to be significantly larger than the stresses measured within the particles. This is hypothesized to be due to the use of rigid confining walls versus the flexible membrane employed by Cui et. al (2007). In the tightly compacted specimen, the resultant forces measured at the rigid confining walls can be influenced by a single highly stressed particle. Thus, the boundary stress measured at the wall can be significantly larger than the average stress of the particulate assembly.

Micro-scale properties influencing macro-scale response include normal, tangential, and rolling stiffness, local friction, and non-dimensional plastic coefficient at the contacts (Belheine et al. 2009). Particle stiffness, assembly fabric, and shear history determine the distribution of forces within a particulate system (Antony 2000). The influence of particle properties to include specific gravity, contact stiffness, surface friction, and rolling resistance were examined in this study. Values of specific gravity ranged

from 0.9 to 7.8, values of contact stiffness ranged from 10,000 to 1,200, values of surface friction ranged from 0.3 to 0.5, and a rolling resistance value of 7.0 was applied to the simulated sand particles to account for the use of spherical particles to model non-spherical materials. All of the applied properties greatly influenced the behavior of the modeled materials and enabled reasonable replication of laboratory testing of physical specimens.

Forces are transmitted in well-graded specimens through systems of force chains versus well distributed in uniformly graded specimens (Evans et al. 2009). Antony (2000) observed that normal contact forces can be subdivided into those carrying less than the average and those carrying more. While these findings are well accepted for physical specimens, these behaviors were not observed in this study. The selection of bimodal particle sizes, 0.80- and 0.20-in.-diameter particles, and the specimen size did not allow for the formation of well-established force chains. The 1:4 large particle to small particle diameter size ratio was not sufficient to allow the small proportion particles to fit into the void between contacting large particles. This prevented the short-circuiting of the small proportion, requiring the entire particle assembly to share the applied stresses. Additionally, the large particle diameter to specimen size ratio of 1:5 was not sufficient to allow for the formation of force chains.

6.2.1 Distribution of stresses

The distribution of shear stresses presented in Figure 31 through Figure 33 show the average shear stress within each particle-size fraction. However, to understand the contribution of each particle-size fraction to the strength capability of the entire specimen, the volume of each particle must also be considered. To capture the contribution of each particle fraction to the entire assembly strength, the stress porosity was considered. In this technique the stress within each particle is weighted based upon its volume according to Equation 28 and averaged across each particle-size fraction. Figure 34 through Figure 36 show the stress porosity for the stainless steel, polypropylene/stainless steel, and sand/silty-clay bimodal assemblies respectively. A clear transition in material behavior is not apparent for the assemblies containing the spherical particles. However, the assemblies of sand/silty-clay show increasing stress porosity for the large material as the proportion is increased.

Figure 34. Stress porosity of stainless steel specimens at 15 psi (left) and 50 psi (right) confining pressure.

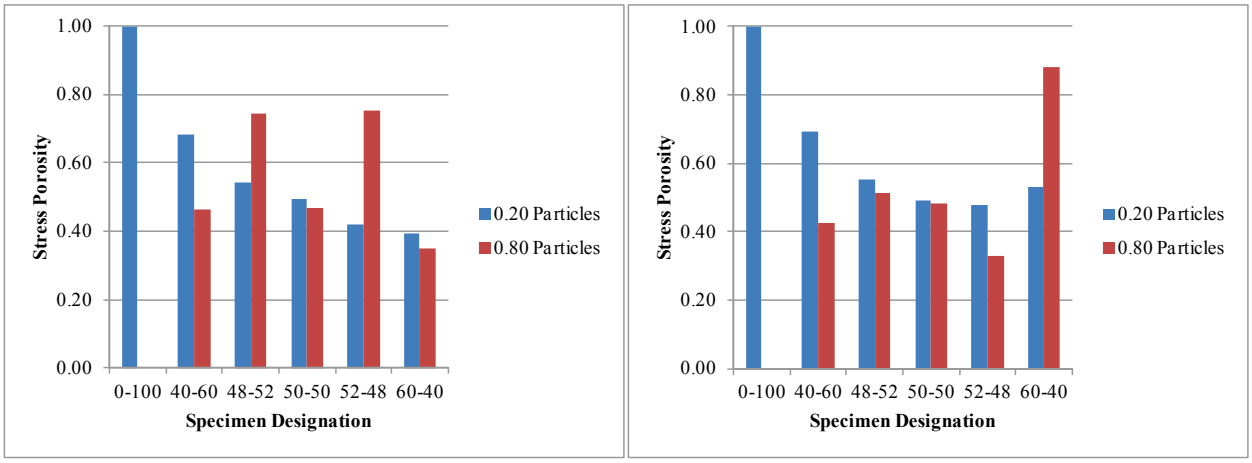

Figure 35. Stress porosity of polypropylene/stainless steel specimens at 15 psi (left) and 50 psi (right) confining pressure.

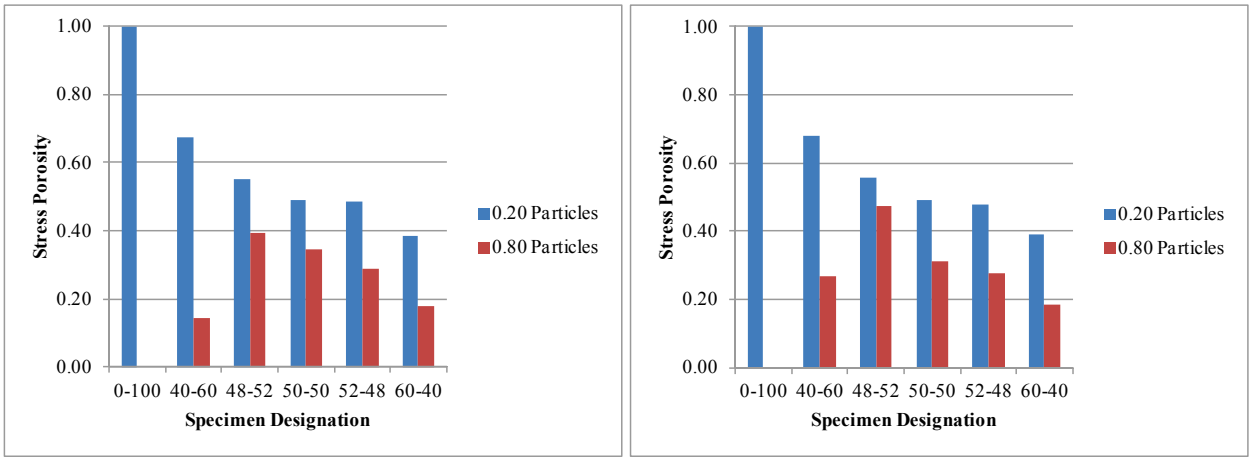

Figure 36. Stress porosity of sand/silty clay specimens at 15 psi (left) and 50 psi (right) confining pressure.

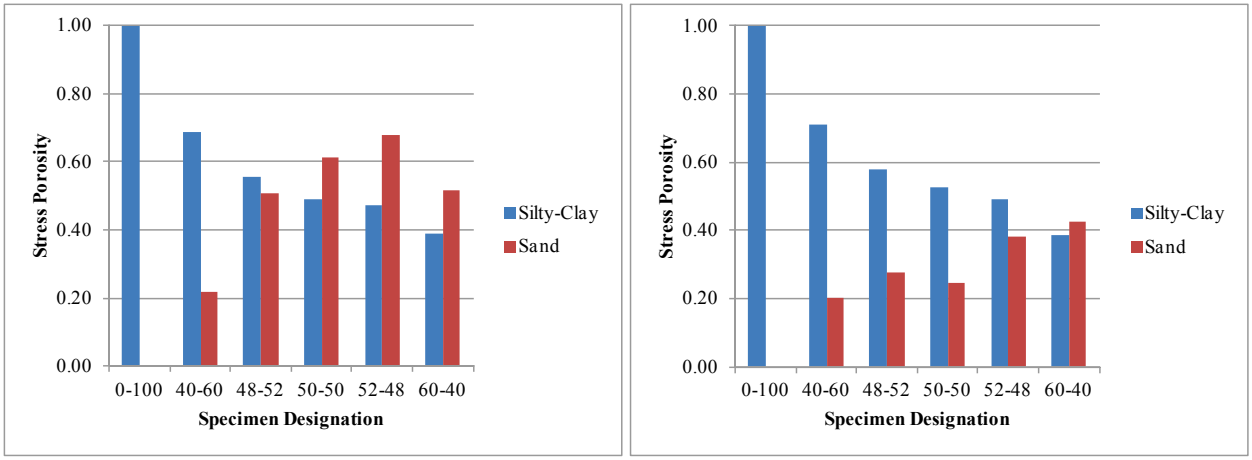

$$n_{\sigma} = \frac{\sum_{i=1}^{N} \left(\frac{V_p}{V_s} \sigma_{particle\ shear} \right)}{\sigma_{average\ shear}} \quad (28)$$

where:

n_{σ} = shear stress porosity

N = number of particles in a discrete size fraction

V_p = volume of a particle

V_s = solids volume of the assembly

$\sigma_{particle\ shear}$ = shear stress within a particle

$\sigma_{average\ shear}$ = average shear stress of the assembly

6.2.2 Coordination number

Coordination number describes the average number of contacts for the particles in the assembly (Bathurst and Rothenburg 1988). Particulate materials transmit loads through shared contacts. Coordination number strongly influences the behavior of particulate materials because increased coordination number results in more uniform distribution of loads. O'Sullivan et. al (2006) observed decreased strength accompanied a reduction in average coordination number. The critical coordination number reflects a minimum requirement for physical stability (Thornton 2000). A coordination number of approximately 6, for dense assemblies, or 4, for loose assemblies, indicates the required contacts for stability have been achieved and the system effectively locks up. When the critical coordination number is reached, significant volume change is observed. Coordination number greatly influences shear displacement with increasing number of contacts limiting particle rotation. Assemblies with coordination numbers less than 3 are unstable. As coordination number reaches its maximum value of 6, particles are restrained to a point that rotations practically disappear (Bathurst and Rothenburg 1988).

The critical coordination number described by Bathurst and Rothenburg (1988) describes uniform assemblies of rigid spheres. The coordination number for the uniform assemblies of spheres examined in this study exceeded the proposed maximum value of 6. Cui et. al (2007) indicated

that the initial coordination number for polydisperse specimens is lower than monodisperse specimens despite lower void ratio. This relationship was not observed in this study. The void ratio for the bimodal numerical specimens generated as part of this study were lower that uniform assemblies, but also exhibited greater initial coordination number.

During triaxial compression testing, the coordination number decreased slightly for the bimodal distributions, but more significantly for the uniform assemblies. Although the specimen coordination number stabilizes after 3 percent strain, the coordination number within the specimen continually changes with some regions increasing and others decreasing (Cui et. al 2007). After an initial rearrangement, the particle matrix in granular systems remains constant. Shearing, or change in stress ratio, results in reduced coordination number (Sitharam et. al 2002). The change in coordination number of the stainless steel, polypropylene/stainless steel, and sand/silty-clay bimodal specimens between 0 and 5 percent shear strain is presented in Tables 14 through 16, respectively.

During shearing, particles contributing in force chains undergo continuous cycles of compression and relaxation without a change in coordination number (Antony 2000). Although small changes in coordination number for the assembly are measured, particles participating in force chains may have increasing coordination numbers that are offset by the reduced coordination number of the non-contributing particles in the assembly. O'Sullivan et. al (2004) observed that traditional measures of fabric such as coordination number are not effective for distinguishing differences in mechanical performance. While coordination number may not be effective for determining the formation and evolution of force chains, results of this study indicate that total coordination number correlates well with observed mechanical performance. For similar composing materials, increased values of coordination number corresponded with increased shear strength. The shear stress and coordination number at 5 percent shear strain were plotted for the stainless steel, polypropylene/stainless steel, and sand/silty-clay bimodal blends investigated in this study in Figure 37 and Figure 38. A clear linear trend between total coordination number and shear stress is apparent.

Table 14. Change in coordination number during shear of stainless steel specimens.

Particle Fraction % (coarse to fine)	15 psi			50 psi		
	CN 0% ε_{shear}	CN 5% ε_{shear}	ΔCN	CN 0% ε_{shear}	CN 5% ε_{shear}	ΔCN
0-100	6.2	5.7	-8.9%	6.6	5.9	-10.6%
40-60	6.6	6.5	-0.9%	8.5	8.5	-0.6%
48-52	7.3	7.2	-0.4%	8.5	8.5	-0.3%
50-50	7.6	7.6	-0.5%	8.6	8.5	-1.1%
52-48	6.7	6.6	-1.1%	8.8	8.7	-1.0%
60-40	8.0	7.7	-3.6%	8.1	7.8	-3.6%

Table 15. Change in coordination number during shear of polypropylene/stainless steel specimens.

Particle Fraction % (coarse to fine)	15 psi			50 psi		
	CN 0% ε_{shear}	CN 5% ε_{shear}	ΔCN	CN 0% ε_{shear}	CN 5% ε_{shear}	ΔCN
0-100	6.2	5.7	-8.9%	6.6	5.9	-10.6%
40-60	6.8	6.6	-1.8%	8.5	8.5	-0.2%
48-52	7.7	7.7	-0.1%	8.8	8.7	-0.8%
50-50	7.8	7.7	-0.5%	8.5	8.5	-0.5%
52-48	8.8	8.7	-1.3%	8.9	8.8	-1.2%
60-40	8.2	7.9	-3.5%	8.2	7.9	-3.4%

Table 16. Change in coordination number during shear of sand/silty clay specimens.

Particle Fraction % (coarse to fine)	15 psi			50 psi		
	CN 0% ε_{shear}	CN 5% ε_{shear}	ΔCN	CN 0% ε_{shear}	CN 5% ε_{shear}	ΔCN
0-100	7.1	6.2	-13.9%	8.2	8.2	0.0%
40-60	8.1	8.1	-0.2%	9.2	9.1	-0.9%
48-52	8.5	8.5	-0.2%	9.6	9.5	-0.8%
50-50	8.4	8.4	-0.4%	9.5	9.4	-1.1%
52-48	8.7	8.6	-0.7%	9.4	9.3	-1.0%
60-40	8.6	8.3	-3.0%	8.7	8.4	-2.9%

Figure 37. Influence of coordination number on shear strength of specimens sheared at 15-psi confining pressure.

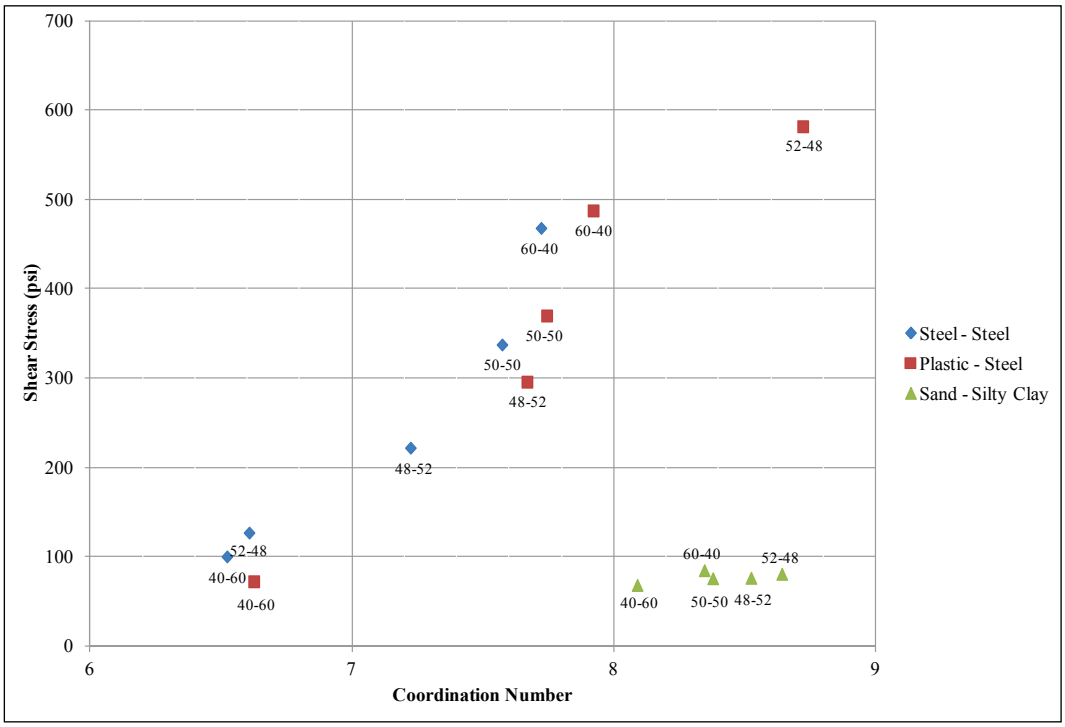

Figure 38. Influence of coordination number on shear strength of specimens sheared at 50-psi confining pressure.

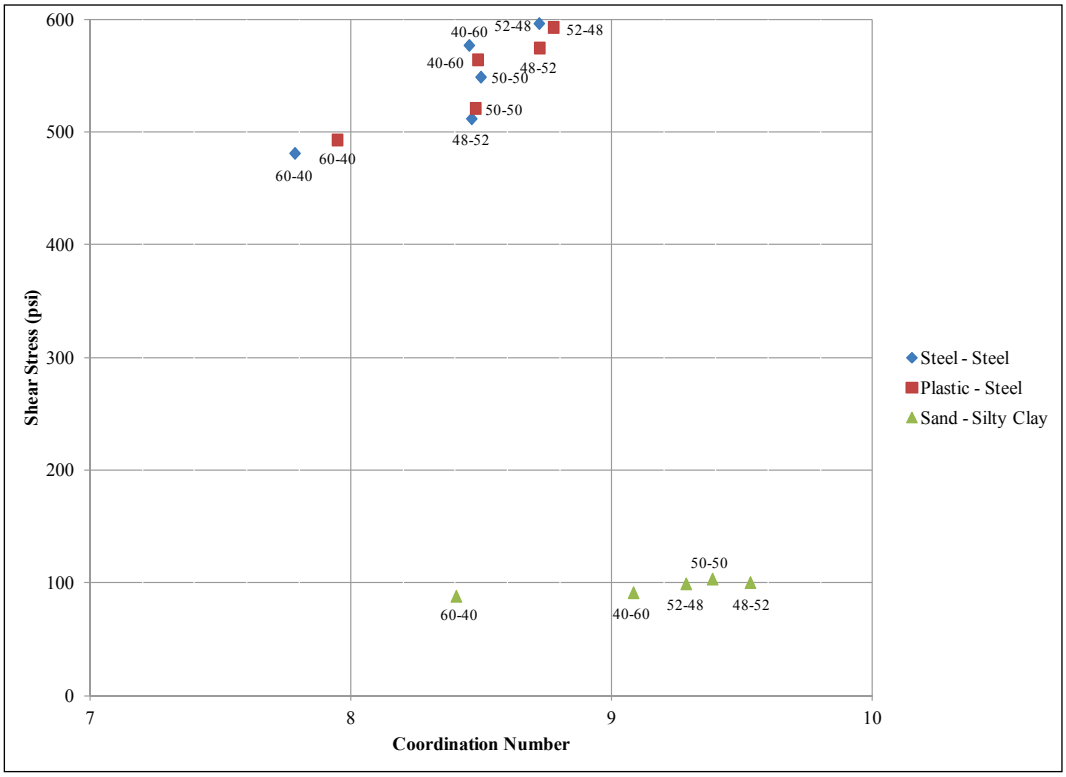

7 Summary and Conclusions

The influence of particle-size distribution on the stress transfer mechanisms occurring in bimodal particulate materials was investigated in this study. A serial version of the 3-D DEM model developed by Horner et.al (2001) was used to simulate the consolidated-undrained triaxial compression testing of cubical specimens. The DEM model was calibrated using laboratory tests on assemblies of uniform spheres composed of stainless steel, polypropylene, sand, and silty-clay materials. Calibrated material properties were developed by comparing the stress-strain behavior of simulated tests to the results obtained in the laboratory. Once calibrated, the model was used to simulate triaxial testing on bimodal specimens composed of 0.80- and 0.20-in.-diam spheres. The stress-strain response of specimens subjected to simulated triaxial compression testing compared favorably to the relationships observed in laboratory testing.

The primary advantage to employing numerical testing techniques as compared to traditional laboratory testing is the availability of micro- or particle-scale data. Data obtained from the DEM in this study included individual particle and particle-size fraction average stresses and coordination number. Distinct changes in behavior resulting from changes in particle-size fractions were not observed. However, a relationship between coordination number and specimen stiffness was observed. Coordination number describes the average number of contacts for each particle within a compacted assembly. Coordination number is influenced by a number of factors to include particle shape, surface friction, size ratio, and assembly density. The density is strongly influenced by the proportion of particle sizes composing the assembly and therefore, particle-size fraction has an indirect effect on the shear strength of particulate materials.

The central theme of this work was related to percolation theory as described in Peters and Berney (2010). Percolation theory describes the critical connectivity within a network. The point at which the critical connectivity is reached is the percolation threshold. With respect to bimodal particulate materials, the exhibited behavior is controlled by the dominant size fraction. As the subordinate fraction is increased, the percolation

threshold is reached, and the behavior transitions from being dominated by one fraction to the other. Peters and Berney (2010) observed erratic and even unstable behavior in blends of sand and silty-clay at the percolation threshold. Once the percolation threshold is reached in a fine/coarse bimodal system, sufficient connectivity exists for the formation of force chains. The development of force chains results in stress localization and short-circuiting of the fine proportion.

The percolation threshold was investigated in this study by examining bimodal distributions that were dominated by one fraction or were approaching the percolation threshold. The investigated blends included 0-100, 40-60, 48-52, 50-50, 52-48, and 60-40 (coarse-fine) content by volume percentage. Additionally, the influence of material type on the critical particle-size proportions was investigated by examining blends of stainless steel only, less stiff large fraction composed of polypropylene blended with small stainless steel, and less stiff small fraction in the blends of sand and silty-clay as presented in Peters and Berney (2010). Distinct changes in behavior resulting from changes in particle-size fraction were not observed in this study with the exception of the sand/silty-clay blends tested at a confining pressure of 15 psi. The stress-strain behavior of these blends transitioned from resembling a uniform assembly of fine particles to a uniform assembly of coarse particles with increasing coarse material proportion. Although no definite transitional proportion was identified, the theory of percolation was validated for the particulate materials observed in this study. The objective of this investigation was to examine the influence of particle-size distribution on the stress transfer mechanisms of bimodal particulate assemblies. Both physical and numerical methods were employed. The physical specimens showed definite changes in stress-strain behavior resulting from changes in particle-size distribution. However, the expected increases and decreases in strength based on large particle proportion was not observed principally due to the limiting number of particles used within the DEM simulation which allowed boundary conditions to influence the overall constitutive response. The stress-strain behavior of the numerical specimens differed both from expectation and from the observed laboratory performance. However, a relationship between coordination number and assembly stiffness was observed. Particulate materials transmit loads at the shared contact points. For the bimodal assemblies investigated in this study, an increase in contacts resulted in greater sharing of loads as indicated by greater strength and stiffness, resulting in more efficient stress transfer.

Factors contributing to increased contacts or coordination number can also contribute to increased stiffness and strength.

Key findings from this investigation include:

- DEM is an effective tool for investigating the micromechanics driving macro-scale performance in particulate materials.
- Careful calibration is required to model materials of interest using DEM models.
- Differences in observed behavior between physical and numerical experimentation methods are owing to the formulation of the numerical model. While not all issues can be addressed, careful modeling of the physical system results in good agreement between physical and numerical methods.
- The existence of a distinct percolation threshold was not observed in this investigation.
- The behavior of both physical and numerical specimens with changing particle-size fractions differed from expectations.
- While no direct relationship between particle-size distribution and macro-scale behavior were observed, a distinct relationship between coordination number and stress-strain behavior was documented.
- The domain size of the DEM of 7,000 particles was likely not sufficient to elicit the percolation response in the particle systems. A larger domain size would reduce boundary influences and allow for a clearer evaluation of particle response.

Recommendations resulting from this work include:

- Further investigation is required to quantify the influence of modeled features to include rigid walls and cubical specimens.
- Further development of the Horner, Peters, and Carrillo (2010) model is required to include the use of flexible membrane and pore water fluid.
- Additional testing is required on non-spherical particles to examine the validity of the coordination number and stress-strain behavior relationship in naturally occurring particles.
- Use of a larger particle domain size to enable percolation responses to develop. This will require greater computer processing power and parallelization of the DEM code to optimize run times.

References

Antony, S. 2000. Evolution of force distribution in three-dimensional granular media. *Physical Review E* 63(1):1-13.

Armstrong, J. C., and W. A. Dunlap. 1966. *The use of particulate mechanics in the simulation of stress-strain characteristics of granular materials*. Texas Highway Department, Research Report 99-1. College Station, TX: Texas Transportation Institute.

ASTM International. 2004. Standard test method for consolidated undrained triaxial compression test for cohesive soils. Standard D4767.West Conshohocken, PA: ASTM International.

Bardet, J. P. 1998. Introduction to computational granular mechanics. In *Behaviour of granular materials* ed. B. Cambou, 99-169. New York: Springer-Verlag Wien.

Bathurst, R. J., and L. Rothenburg. 1988. Micromechanical aspects of isotropic granular assemblies with linear contact interactions. *Journal of Applied Mechanics* 55(1):17-23.

Belheine, N., J.P. Plassiard, F.V. Donzé, F. Darve, and A. Seridi. 2009. Numerical simulation of drained triaxial test using 3D discrete element modeling. *Computers and Geotechnics* 36(1-2):320-331.

Carrillo, A. R., D. A. Horner, J. F. Peters, and J. E. West. 1996. Design of a large scale discrete element soil model for high performance computing systems. In *Proceedings of the 1996 ACM/IEEE Conference on Supercomputing (CDROM) – Supercomputing '96,* 1-15. New York: ACM Press.

Cavarretta, I., M. Coop, and C. O'Sullivan. 2010. The influence of particle characteristics on the behavior of coarse grained soils. *Géotechnique* 60(6):413-423.

Christoffersen, J., M. M. Mehrabadi, and S. Nemat-Nasser. 1981. A micromechanical description of granular material behavior. *Journal of Applied Mechanics* 48(2): 339.

Cui, L., and C. O'Sullivan. 2006. Exploring the macro- and micro-scale response of an idealized granular material in the direct shear apparatus. *Géotechnique* 56(7): 455-468.

Cui, L., C. O'Sullivan, and S. O'Neill. 2007. An analysis of the triaxial apparatus using a mixed boundary three-dimensional discrete element model. *Géotechnique* 57(10):831-844.

Cundall, P. A. 1974. Rational design of tunnel supports: A computer model for rock mass behavior using interactive graphics for the input and output of geometrical data. Technical Report MRD-2-74. Department of the Army, Corps of Engineers. Omaha, NE: Missouri River Division.

Cundall, P. A., and O. D. L. Strack. 1979. A discrete numerical model for granular assemblies. *Géotechnique* 29(1):47-65.

Das, B. M. 2010. *Principles of geotechnical engineering* (7th ed.). Stamford, CT: Cengage Learning.

Deng, A., and Y. Xiao. 2010. Measuring and modeling proportion-dependent stress strain behavior of EPS-sand mixture. *International Journal of Geomechanics* 10(6): 214-222.

Evans, T. M., H. Mojarrad, C. Cunningham, and A. A. Tayebali. 2009. Grain size distribution effects in 2D discrete numerical experiments. In *Contemporary topics in in situ testing, analysis, and reliability of foundations (GSP 186)*, ed. M. Iskander, D. F. Laefer, and M. H. Hussein, 58-65. ASCE.

Feda, J. 1982. Mechanics of particulate materials: The principles. In *Developments in geotechnical engineering* 30. New York: Elsevier Scientific Publishing Company.

Hitcher, P.Y. 1998. Experimental behavior of granular materials. In *Behaviour of granular materials*, ed. B. Cambou, 1-97. New York: Springer-Verlag Wien.

Horner, D. A., J. F. Peters, and A. R. Carrillo. 2001. Large scale discrete element modeling of vehicle-soil interaction. *Journal of Engineering Mechanics* 127(10):1027-1032.

Jiang, M., and H. Yu. 2006. Application of discrete element method to geomechanics. In *Modern trends in geomechanics*, ed. W. Wu and H.-S. Yu, 241-269. New York:Springer.

Kuo, C.-Y., and J. D. Frost. 1997. Initial fabric and uniformity of a sand specimen—An image analysis approach. In *Mechanics of deformation and flow of particulate materials*, ed. C. S. Chang, A. Misra, R. Y. Liang, and M. Babic, 214-223. New York: ASCE.

McGeary, R. K. 1961. Mechanical packing of spherical particles. *Journal of the American Ceramic Society* 44(10):513-522.

Ng, T.T. 2009. Discrete element method simulations of the critical state of a granular material. *International Journal of Geomechanics* 9(5):209-216.

Oda, M., and K. Iwashita, ed. 1999. *Mechanics of granular materials: An introduction*. Rotterdam: A. A. Balkema.

O'Sullivan, C. 2002. The application of discrete element modelling to finite deformation problems in geomechanics. PhD diss., University of California, Berkeley.

O'Sullivan, C., J. D. Bray, and L. Cui. 2006. Experimenal validation of particle-based discrete element methods. In *GeoCongress 2006*, 1-18. ASCE.

O'Sullivan, C., J. D. Bray, and M. Riemer. 2004. Examination of the response of regularly packed specimens of spherical particles using physical tests and discrete element simulations. *Journal of Engineering Mechanics* 130(10):1140-1150.

Peters, J. F., and E. S. Berney. 2010. Percolation threshold of sand-clay binary mixtures. *Journal of Geotechnical and Geoenvironmental Engineering* 136(2):310-318.

Shearer, M., and D. G. Schaeffer. 1997. Stress fluctuations in granular materials. In *Mechanics of deformation and flow of particulate materials,* ed. C. S. Chang, A. Misra, R. Y. Liang, and M. Babic, 259-267. New York: ASCE.

Sitharam, T. G., S. V. Dinesh, and N. Shimizu. 2002. Micromechanical modeling of monotonic drained and undrained shear behavior of granular media using three-dimensional DEM. *International Journal for Numerical and Analytical Methods in Geomechanics* 26(12):1167-1189.

Thornton, C. 2000. Numerical simulations of deviatoric shear deformation of granular media. *Géotechnique* 50(1):43-53.

Vallejo, L. E. 2001. Interpretation of the limits in shear strength in binary granular mixtures. *Canadian Geotechnical Journal* 38(5):1097-1104